CHALMERS
UNIVERSITY OF TECHNOLOGY

Ion runaway in magnetized plasmas

Thesis for the degree Master of Science in Physics and Astronomy

Ola Embréus

Department of Applied Physics
CHALMERS UNIVERSITY OF TECHNOLOGY
Gothenburg, Sweden 2014

Ion runaway in magnetized plasmas
OLA EMBRÉUS

Department of Applied Physics
Chalmers University of Technology
SE-412 96 Göteborg
Sweden
Tel: +46 (0) 31 772 1000

Ion runaway in magnetized plasmas

Ola Embréus
Department of Applied Physics
Chalmers University of Technology

Abstract

It has been suggested that ions accelerated by static electric fields (so-called runaway ions) in magnetized plasmas could explain experimental observations of heavy ion abundances in solar flares and excitation of Alfvénic instabilities during disruptions in fusion plasmas. However, limitations of previous analytic work have prevented definite conclusions. This has motivated a numerical study of the ion kinetic equation with strong electric fields in magnetized plasmas.

In this work the numerical tool CODION (COllisional Distribution of IONs) is developed. It builds upon the existing code CODE, a solver of the electron kinetic equation. CODION solves the initial value problem for the 2-dimensional non-relativistic linearized Fokker-Planck equation in velocity space with a spectral-Eulerian discretization scheme, allowing arbitrary plasma composition and explicitly time-varying electric fields and background plasma parameters.

The model is applied to a range of physical scenarios, and 2D ion velocity space distribution functions have been obtained. In particular, the model has been applied to investigate under which conditions ions will be accelerated in fusion plasmas characteristic for the TEXTOR, JET and ITER tokamaks. Typical time scales and required electric fields for ion acceleration have been determined for various plasma compositions, ion species and temperatures, and the potential for toroidal Alfvén eigenmodes (TAE) to be excited during disruptions considered. The effect on ion acceleration of various models for self-collisions has been investigated.

Results show that during standard operation of fusion experiments, ions will not be accelerated by the runaway mechanism. During typical disruptions it is shown that ions are unlikely to be accelerated, although it could potentially happen under unusual circumstances. It is shown that experimentally observed TAE activity can not be explained by the ion runaway mechanism considered in this work. The utility of CODION for heavy ion acceleration in solar flares is demonstrated, with acceleration rates of various ion species evaluated for one representative scenario.

Keywords: plasma, ion acceleration, runaway, tokamak, fusion, solar flare

Contents

Acknowledgements

I will first attempt to express my gratitude toward Sarah Newton at Culham Centre for Fusion Energy, who has been with me on this ride from the beginning. Always open for discussion and giving a helping hand, she has been immensely helpful throughout this entire period with everything from proofreading to indulging in long discussions about the intricacies of ion acceleration. I am very grateful for her hospitality during my research visit to Culham, and for having been a fantastic supervisor, guide, teacher and friend.

I should further acknowledge the mastermind behind this project, Tünde Fülöp. Her steady optimism about this whole idea, her encouragements and her guidance has allowed me to push ever on without faltering.

It is with gratefulness I acknowledge my supervisor, Dr. Eero Hirvijoki. Ever open to discuss physics of any kind[1], he has helped me keep my spirits up and my mind healthily distracted from the task at hand. I have learnt a lot from my interactions with him, and life in the office would not have been the same without him.

I wish to deeply thank everyone in the eFT group here on Chalmers – Adam, Eero, Albert, István and Tünde – for the welcoming atmosphere and the stimulating environment they have provided during this year. It has been an absolute joy to work alongside and with you all. Huge thanks for the help in proofreading the thesis, for sharing your ideas on ways to improve the presentation and for discussing all the small things that appear during the process. Also, hats off to Geri for tearing my work apart in such a delightful way, providing invaluable feedback for the thesis. I would like to thank Joan Decker for all the fruitful discussions during his stay here at Chalmers.

Finally I wish to thank my partner Brita and my pet spider Gunnar, who have at times been undeservedly[2] neglected because of long hours and late nights spent on this degree project. I am filled with gratitude for your unfaltering support, your encouragements, love and entertaining climbing around on the walls.

Ola Embréus, Gothenburg, December 31, 2014

[1] Dare I say, in particular Lie transform methods of guiding center motion?

[2] ...perhaps not Gunnar

Chapter 1

Introduction

Plasmas are encountered in everyday life. For example, plasmas are generated in fluorescent lamps, and sparks due to static electricity consist of a brief plasma column. They also play a key role in natural phenomena such as the northern lights (aurora borealis). In fact, the majority of ordinary matter in the Universe is in the plasma state, and the study of astrophysical plasmas is a large field of research. In the various applications of plasma physics, the densities and temperatures of the plasma range over almost 30 and 10 orders of magnitude, respectively. In the different parameter regimes, the behaviour of the plasma can be widely different, as are the theoretical approaches to model these systems.

After solids, liquids and gases, plasmas form a fourth state of matter in which the atoms are ionized. This has the consequence that there are free charges in the plasma, generating electromagnetic fields with their motion according to Maxwell's equations. These electromagnetic fields will in turn affect the motion of the particles that generated them, creating a complex and rich interplay giving rise to a wide range of plasma phenomena.

In this chapter we will discuss an important motivation for the study of plasma physics: fusion energy. This will also provide a useful background to the main application of the work undertaken.

1.1 Fusion energy

The ambition of fusion energy research is to develop controlled extraction of energy from nuclear fusion reactions. The binding energy per nucleon is a non-monotonic function of nucleus mass – it is an increasing function at small mass, and a decreasing function at large mass. This has the consequence that energy is released in nuclear reactions where light nuclei combine into heavier ones, or where heavy nuclei split into lighter ones. The former are fusion reactions, while the latter corresponds to fission.

The fission reaction has already been used for decades to produce energy on a large scale; mainly because the activation energy required to initiate a nuclear fission reaction is low. This is partly due to the fact that the reaction is initiated by an incident neutron, a neutral particle which does not interact with the nucleus until it passes within the range of the strong interaction, $\sim 10^{-15}$ m.

On the other hand, while fusion reactions also require the light nuclei to pass within the range of the strong interaction, in this case there are two positively charged particles involved which also interact via the long-ranged Coulomb interaction. To overcome the repulsive Coulomb barrier, one can estimate that the kinetic energy needed is of order

$$E_K = \frac{e}{4\pi\varepsilon_0 r} \sim 1 \text{ MeV} \tag{1.1}$$

for singly charged ions with a distance $r \sim 10^{-15}$ m. For this to happen spontaneously, i.e. by particles in thermal equilibrium, temperatures of order 1 MeV are needed[1]. However, tunneling allows the potential barrier to be penetrated already for temperatures of order $T \sim 10\,\text{keV}$ (corresponding to a hundred million degrees Kelvin) [1] .

Herein lies the complication of fusion energy: how can one raise the temperature of a plasma to millions of Kelvin, for long enough that significant amounts of fusion reactions can take place and in such a way that the energy may be extracted for electricity production?

1.2 Fusion reactor concepts

The theoretical principles behind nuclear fusion are well established – our own Sun is an example of a fusion reactor. However, in the Sun the sheer gravitational pressure both heats the plasma and keeps it confined; this method can obviously not be used in the laboratory. Instead we have to find other ways to contain and heat the plasma. Two main ideas have been pursued in the scientific community: inertial confinement fusion (ICF) and magnetic confinement fusion (MCF).

The idea behind ICF is to heat up a solid pellet – of some suitable material – at a high enough rate that the necessary conditions for fusion reactions to take place are met before the pellet disintegrates. This is usually accomplished by irradiating a small spherical target with multiple high-powered lasers, heating it uniformly to a hundred million Kelvin with such intensity that the pellet is compressed to a volume thousands of times smaller than the initial one [2]. The state-of-the-art facility in this branch of fusion research is the National Ignition Facility (NIF) in the US, where it has been demonstrated that fusion reactions can be initiated using this concept [3].

Strong magnetic fields can be used to confine charged particles, forming the basis for MCF. Many large experiments are active around the world based on this concept and applications to the tokamak scheme for MCF are considered in this thesis. Therefore underlying concepts of tokamak devices are discussed in more detail in the following section. Great technological challenges remain to make either concept viable from a commercial energy production point of view, and there is a large demand for further development of the physics and engineering knowledge in order to make commercial fusion energy production a reality.

1.3 Tokamak physics

The idea behind magnetic confinement is that a charged particle moving in a magnetic field will gyrate around the magnetic field line in a circular motion with radius

$$r_L = \frac{mv_\perp}{|qB|}, \tag{1.2}$$

where m is the mass and q the charge of the particle, $v_\perp$ its velocity perpendicular to the magnetic field and B the magnetic field strength. For a plasma in thermal equilibrium at temperatures required for fusion reactions to occur, this length is of the order tenths of a millimeter for electrons and millimeters to centimeters for ions, at a characteristic magnetic field of 1 T. This indicates that a reactor needs to be of size on the order of meters and have a magnetic field of order Teslas in order to keep a plasma confined.

[1] We follow the plasma physics convention of giving temperatures in energy (eV), i.e. using units where the Boltzmann constant $k_B = 1$.

However, a reactor cannot be straight and infinite, and the solution in magnetic confinement concepts is to bend the plasma into the shape of a closed loop. A large part of the fusion research programme is focused on the tokamak device, in which the plasma configuration is a simple torus.

When one takes into account electric forces and inhomogeneities of the magnetic field that naturally arise in a toroidal geometry ($B \propto 1/R$), it is found that the gyrating orbits will drift across the magnetic field. To prevent loss of confinement, a twist of the magnetic field lines is needed to make the drifting motion cancel out on average. In a tokamak, the so-called poloidal magnetic field component (illustrated in figure 1.1) that twists the field lines is generated by driving a strong toroidal current in the plasma. In larger devices, and future fusion reactor concepts, the required plasma current is of the order several MA. A toroidal magnetic field configuration with twisted field lines is shown in figure 1.1.

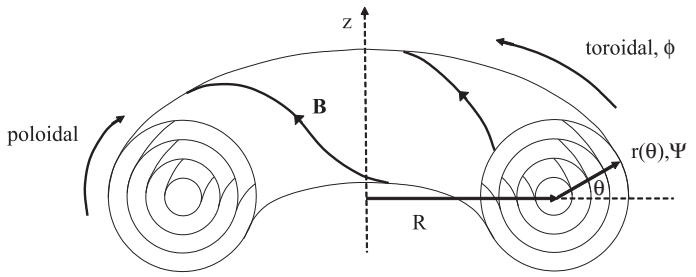

Figure 1.1: An illustration of a toroidal geometry, demonstrating the conventional toroidal and poloidal angles.

1.3.1 Alfvén waves

A simplified description of plasmas can be obtained by taking integral moments of the equations of motion of the particle species in the plasma, considering only average quantities such as density and flow velocity. Together with Maxwell's equations, this provides a set of equations taking the form of those for a conducting fluid in a magnetic field, known as the magnetohydrodynamic (MHD) equations. This framework has been successful in describing realistic equilibrium plasma configurations [1]. Considering small perturbations from such an equilibrium, allowing a linearization of the MHD equations, one can find wave solutions – plasma waves.

In a uniform plasma, one obtains the characteristic shear Alfvén wave, a transverse oscillation of the plasma moving along the magnetic field-lines with phase velocity $v_A = B/\sqrt{\mu_0 \rho}$, where ρ is the mass density of the plasma. This wave requires only a low energy input to be excited since it does not induce compression of the plasma, and it is therefore well-known to be associated with instabilities in both fusion and space plasmas.

In a non-uniform plasma B and ρ_0 vary with position, forming a continuous Alfvén spectrum where a wave of given frequency can be excited at a specific location. In more complex geometries, different wave modes couple to each other, allowing gaps to form in the Alfvén spectrum. The amplitude of a wave-mode in a tokamak takes the form $A = A_{mn} e^{i(n\phi - m\theta)}$, where θ and ϕ are the poloidal and toroidal angles respectively, and (m, n) the mode numbers. Toroidicity introduces a $\cos\theta$-dependence to the magnetic field strength, causing m-modes to couple with $m+1$-modes, forming band gaps[2] in the Alfvén

[2]Analogous to the formation of band gaps in semiconductors

spectrum at certain radii in which a discrete wave mode resides – the toroidal Alfvén eigenmode (TAE) [4, 5, 6].

It is well known that energy is not conserved individually in Maxwell's equations or the kinetic equation governing the evolution of particles, but only in the combined set of equations [7]. This implies the possibility of energy transfer between particles and radiation field. In plasmas, it is found that a resonant interaction between wave modes and particles can occur, allowing discrete wave modes to be excited by the presence of energetic particles with velocity in resonance with the phase velocity of the wave [8]. Fast particle populations from various sources are often present in tokamaks. In the next two sections the generation of these populations by acceleration in an electic field will be described. The resonant excitation of TAE instabilities by such populations will then be the focus of section 4.2.

1.3.2 Electron runaway

Electron runaway is a phenomenon with the potential to critically damage tokamaks [citation needed]. Runaway can happen during disruptions – events where the plasma is suddenly terminated. In these events the plasma is rapidly cooled, causing the plasma resistivity to increase as it is inversely proportional to temperature. Here, the plasma resistivity η is given in terms of the relation $E = \eta j$, where j is the plasma current and E the electric field. Since the temperature during these events drops at a much higher rate than the decay rate of the current, large electric fields will be induced. These electric fields may accelerate electrons in the plasma, potentially up to relativistic speeds, and a large fraction of the plasma current can be converted into a highly energetic electron beam. If the beam strikes the wall of the plasma chamber it can cause serious damage to plasma-facing components. Methods to mitigate the generation of runaway electrons are therefore actively being studied.

To understand how electron runaway happens – and by extension provide a useful picture to keep in mind when we turn to ion runaway – we may look at the equations of motion for an electron in the plasma. As will be shown in section 2.4, the total force parallel to the magnetic field acting on an electron in a plasma can approximately be described by

$$F_\parallel = qE_\parallel - \frac{mv_T}{\tau_c} G(v/v_T), \tag{1.3}$$

where v_T is the thermal velocity, τ_c a characteristic collisional time scale and

$$G(x) = \frac{\phi(x) - x\phi'(x)}{2x^2} \tag{1.4}$$

is the Chandrasekhar function, where $\phi(x) = \frac{2}{\sqrt{\pi}} \int_0^x \mathrm{d}x \, \exp(-x^2)$ is the error function. This function determines the friction with other electrons, and increases in proportion to the velocity at low velocities, $G \propto v$, but at high velocities it is a decreasing function, $G \propto 1/v^2$. It has a maximum value near $v/v_T = 1$. This has the consequence that, unless the electric field is strong enough to overcome the collisional friction at all velocities, there are two velocities satisfying the equilibrium condition $F_\parallel(v) = 0$, as demonstrated in figure 1.2.

One solution is found at low velocities and is directly proportional to the electric field. This linear response is an essential part of the description of plasma resistivity. Another solution is found at a high, critical velocity v_c. As effects of collisional velocity space diffusion was neglected in Eq. (1.3), all electrons between these velocities will be decelerated. However, if we consider an electron distribution initially in local thermodynamic

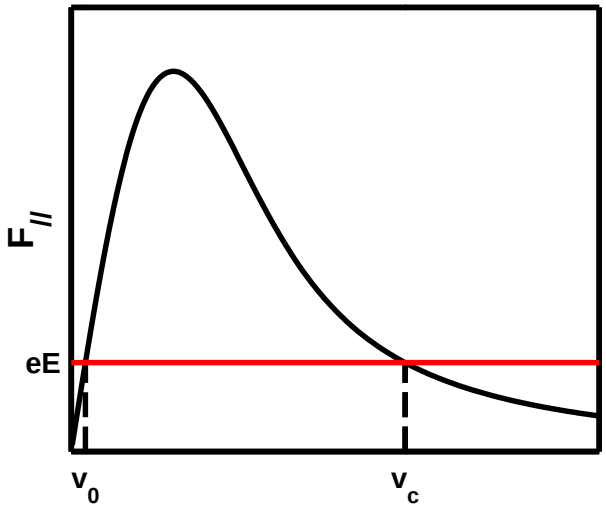

Figure 1.2: Illustration of the velocity dependence of the friction force on an electron in a plasma due to collisions with other electrons (black), together with the force from the driving electric field (red), demonstrating the runaway region $v > v_c$.

equilibrium, its velocity distribution has the Boltzmann form

$$f_e \propto \exp(-v^2/v_T^2). \tag{1.5}$$

In the "tail" of such a distribution there will always be at least a few particles with velocity $v > v_c$, which will be accelerated by the electric field and eventually reach relativistic velocities. These are the runaway electrons. Collisional diffusion will feed lower-velocity electrons into the runaway region ($v > v_c$), so that runaway electrons can be continuously generated as long as the electric field is maintained. In addition, a runaway electron can collide with a slow electron in a so-called knock-on collision, causing both to end up in the runaway region $v > v_c$. This leads to an exponential growth of the runaway density, causing a runaway "avalanche" [9].

Electron runaway becomes a greater threat in larger machines, where the total plasma current available for conversion to runaways is bigger. In future devices, such as ITER, electron runaway is expected to be a critical threat [10].

1.3.3 Ion runaway

Fast ion populations can be generated by a similar mechanism to that producing electron runaway, but the full picture is different. At low velocities the friction between ion species dominates and is of the same form as that for electrons, allowing a similar initial runaway mechanism. However, at higher velocities the collisional friction between ions and electrons will dominate, and will prevent the ions from being accelerated further at the moderate electric field strength of interest in our applications, as further discussed in section 2.4. Thus, the equilibrium $F_{\|} = 0$ has three solutions: a low velocity (describing resistivity), an intermediate runaway threshold velocity v_{c1} similar to the electron v_c, and a high velocity v_{c2} where electron friction limits the ion acceleration. This is demonstrated in figure 1.3. Ions are only accelerated in the $v_{c1} < v < v_{c2}$ region, and the ion velocity distribution tends to develop a "bump" of increased density near $v = v_{c2}$ where all runaway ions eventually accumulate.

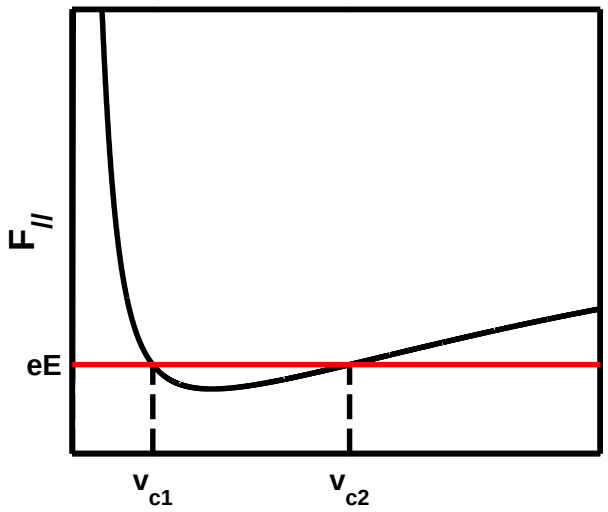

Figure 1.3: Velocity dependence of the friction force on an ion in a plasma due to collisions with other ions (dominant at low velocities) and electrons (dominant at high velocities). The force from the driving electric field determines the runaway region $v_{c1} < v < v_{c2}$.

Acceleration of ions by electric fields has received attention in various contexts. The phenomenon was mentioned as early as 1959 in the context of early fusion experiments [11], where the velocity v_{c2} of runaway ions was calculated from similar considerations as described here. In analytic studies, Gurevich [12] and Harrison [13] considered the rate at which ion runaways are generated both in solar and laboratory plasmas. This was used by Holman [14] to investigate whether abundances of high energy ions in solar flares could be explained by this type of ion runaway mechanism, results being inconclusive due to the limitations of the test-particle model employed and limited available observational data.

Furth and Rutherford [15] investigated the dynamics of the ion distribution using the full drift kinetic equation [16]. They developed the form of the steady state ion distribution using an asymptotic expansion procedure similar to that used in the analytic studies of runaway electrons [17, 18]. Helander *et al.* [19] considered the dynamics which can be produced by short lived fields, and studied the initial value problem, and determined an analytic form for the initial acceleration of the runaway ion distribution. The solution was valid for trace amounts of impurities, small velocities and short times, and the generalization to arbitrary plasma composition was done by Fülöp and Newton [20]. In the last paper, it was also investigated whether the positive velocity gradient of the ion runaway distribution forming near v_{c2} could drive a TAE instability in a tokamak plasma during disruptions. The results were also here inconclusive since the model used to develop the analytic solution was not strictly valid for disruption-type parameters.

The analytic solutions developed in previous work to describe ion runaway are limited in their applicability due to the complexity of the problem. This has motivated the development of a numerical tool to allow detailed study of the time evolution of an ion runaway distribution. The numerical tool ARENA [21] used to obtain the ion distribution in the paper by Helander *et al.* [19] is a numerically expensive 3D Monte Carlo code developed for runaway electron simulations. A significantly numerically less expensive tool CODE was developed, based on a simpler model for the runaway electron problem [22]. In this work the efficient tool CODION (COllisional Distribution of IONs) is developed, building upon the structure of CODE but designed to treat the problem of ion acceleration.

1.4 Outline

The main body of this work is divided into three parts. In Chapter 2 the theoretical description of plasmas is outlined, and the equation of motion (the kinetic equation) for the distribution of ions is derived. Simple analytic estimates of the critical velocities are presented, highlighting the conditions under which ion runaway is expected to be significant. Chapter 3 describes the implementation of the kinetic equation in CODION. In Chapter 4 the model is applied to a variety of physical scenarios, illustrating typical acceleration time scales in laboratory and space plasmas. It is demonstrated that TAEs are unlikely to be excited in tokamaks by ions accelerated by the runaway mechanism described in this work. The work is concluded and an outlook presented in Chapter 5.

Chapter 2

Theoretical description

In this chapter the theoretical elements and approximations used to describe a fully ionized plasma will be outlined. A kinetic equation describing the time-evolution of the statistical ensemble of ions in a plasma will be derived, in the limit where spatial inhomogeneities are negligible. A detailed study of collisions will be presented, and a model for collisions of ions with other particle species in the plasma will be derived. The forces acting on a test-ion in a plasma are obtained from the kinetic equation and will be analyzed, yielding a simple analytic condition for the range of velocities in which a test-ion will be accelerated by an electric field. This will indicate in which parameter regimes acceleration of ions is likely to be significant. The presentation borrows from a range of sources, the main inspiration being the brilliant plasma physics texts [16, 23, 24, 25, 26].

2.1 The kinetic equation

To study the dynamics of a plasma, we introduce the distribution function $f_a = f_a(\mathbf{x}, \mathbf{v})$, which describes the density of a given particle species a in phase space. This is defined such that

$$n_a(\mathbf{x}) = \int \mathrm{d}^3\mathbf{v}\, f_a(\mathbf{x}, \mathbf{v}) \tag{2.1}$$

is the number density of that species in the plasma. We are considering situations where particle number is locally conserved (negligible rate of fusion or other nuclear reactions). If we initially neglect microscopic interactions ("collisions") between particles, we may write the continuity equation for the distribution function in phase space $\mathbf{z} = (\mathbf{x}, \mathbf{v})$,

$$0 = \frac{\partial f_a}{\partial t} + \frac{\partial}{\partial \mathbf{z}} \cdot \Big(\dot{\mathbf{z}} f_a\Big) = \frac{\partial f_a}{\partial t} + \dot{\mathbf{x}} \cdot \frac{\partial f_a}{\partial \mathbf{x}} + \dot{\mathbf{v}} \cdot \frac{\partial f_a}{\partial \mathbf{v}} \equiv \frac{\mathrm{d} f_a}{\mathrm{d}t}, \tag{2.2}$$

where we explicitly used $\nabla \cdot \dot{\mathbf{x}} \equiv \nabla \cdot \mathbf{v} = 0$ and $\nabla_{\mathbf{v}} \cdot \dot{\mathbf{v}} = 0$[1]. With the equations of motion for a particle given by the Lorentz force,

$$\dot{\mathbf{v}} = \frac{q_a}{m_a}\Big(\mathbf{E} + \mathbf{v} \times \mathbf{B}\Big), \tag{2.3}$$

with q_a its charge and m_a its mass, the kinetic equation for the distribution function takes the form

$$\frac{\partial f_a}{\partial t} + \mathbf{v} \cdot \frac{\partial f_a}{\partial \mathbf{x}} + \frac{q_a}{m_a}\Big(\mathbf{E} + \mathbf{v} \times \mathbf{B}\Big) \cdot \frac{\partial f_a}{\partial \mathbf{v}} = 0. \tag{2.4}$$

[1]Note that this latter property is true for the special case of pure electromagnetic forces. Effective forces such as radiative losses do not obey this property [27, 28].

This is the Vlasov equation [29]. The electromagnetic fields here denote the macroscopic fields generated by the charge densities and currents (averaged over some suitable microscopic length-scale)

$$\rho_a = q_a n_a(\mathbf{x}), \tag{2.5}$$

$$\mathbf{j}_a = q_a n_a \mathbf{V}_a \equiv q_a \int \mathrm{d}^3\mathbf{v}\, \mathbf{v} f_a(\mathbf{x}, \mathbf{v}), \tag{2.6}$$

of all species in the plasma, meaning that we have not accounted for the effect of the microscopic fluctuations of the fields that arise due to the motion of the individual particles.

It can be shown that the electric field from a point charge in an overall electrically neutral plasma will be shielded out by the background charges after a distance λ_D, the Debye length. This effect is called Debye screening, and it has the consequence that particles will only interact through microscopic fluctuations with other particles located within a sphere of radius λ_D, the Debye sphere.

With densities and temperatures relevant for controlled fusion experiments, the Debye length is typically less than 10^{-4} m, which is small compared to the overall dimensions of the plasma (meters). One rarely considers phenomena happening on a length-scale smaller than the Debye length in the current context, making it a suitable length-scale over which the distribution function is averaged to make it a smooth function. It is in this sense that one talks about "collisions" in a plasma: the interactions occur within a region small enough to be considered point-wise, compared to all other macroscopic length scales of interest.

Collisions will contribute to the time-evolution of the distribution, and we can write the kinetic equation as

$$\frac{\partial f_a}{\partial t} + \mathbf{v} \cdot \frac{\partial f_a}{\partial \mathbf{x}} + \frac{q_a}{m_a}\Big(\mathbf{E} + \mathbf{v} \times \mathbf{B}\Big) \cdot \frac{\partial f_a}{\partial \mathbf{v}} = C_a\{f_a\}, \tag{2.7}$$

where the collision operator C_a has some functional dependence on the distribution. A particle will interact with all other species b in the plasma, so we may write

$$C_a\{f_a\} = \sum_b C_{ab}\{f_a, f_b\}, \tag{2.8}$$

a sum of the bilinear collision operator over all particle species in the plasma. This introduces the further assumption that the microscopic interactions are well described by separation into pairwise interactions.

2.1.1 2D kinetic equation

We will now reduce the full 6-dimensional kinetic equation given above to a 2-dimensional equation, sufficient for studying the runaway dynamics that will be considered in this work.

A charged particle in a uniform magnetic field will move in a circular (gyro-)motion with constant parallel velocity along the magnetic field, with radius $r_L = mv_\perp/|qB|$ defined in Eq. (1.2), section 1.3. In the case of non-uniform electric and magnetic fields, varying over a characteristic length scale L, it can be shown that perpendicular drifts will be imposed with velocity of order r_L/L slower than the parallel motion along the magnetic field. This fraction is sufficiently small that it is sometimes valid to consider only the parallel motion along the magnetic field.

We will consider primarily plasmas in which the collision frequency (to be defined precisely in section 2.2.2) is also much greater than the characteristic frequency of spatial

variations v_T/L, where v_T is the thermal velocity of the particles. Because of this we will neglect the variation of the system along the parallel direction, leaving us only with velocity space dynamics in the kinetic equation. In this approximation we will not be able to account for toroidal effects in tokamaks such as trapping of particles on the low-field (outer) side of the torus due to the magnetic mirror effect. Methods to simultanously account for both velocity space dynamics and parallel motion have been implemented in various codes, for example LUKE [30] which has been used to model runaway electrons. By doing so the description is complicated considerably, and the resulting equations are numerically more expensive to solve. By restricting ourselves to cases where these effects are negligible, we will obtain a more efficient numerical solver.

In the following we will explicitly show how the kinetic equation under certain conditions can be averaged over one velocity-coordinate to reduce it to a 2-dimensional equation. We have seen that the kinetic equation can be written in the phase-space invariant form

$$\frac{\mathrm{d}f_a}{\mathrm{d}t} \equiv C_a\{f_a\}. \tag{2.9}$$

Introducing a spherical coordinate system (v, θ, φ) in velocity space, using the variable $\xi \equiv \cos\theta$, it takes the form

$$\frac{\partial f_a}{\partial t} + \dot{v}\frac{\partial f_a}{\partial v} + \dot{\xi}\frac{\partial f_a}{\partial \xi} + \dot{\varphi}\frac{\partial f_a}{\partial \varphi} = C_a\{f_a\}. \tag{2.10}$$

Introducing the unit vector

$$\mathbf{b} = \frac{\mathbf{B}}{B}, \tag{2.11}$$

let the coordinate system be locally defined such that the longitudinal (pitch) angle is measured relative to the magnetic field and the azimuthal angle relative to the electric field, i.e.

$$\xi = \frac{\mathbf{v}\cdot\mathbf{b}}{v} = \frac{v_\parallel}{v}, \tag{2.12}$$

$$\cos\varphi = \frac{\mathbf{E}_\perp\cdot\mathbf{v}_\perp}{E_\perp v_\perp}, \tag{2.13}$$

where we have introduced the decomposition $\mathbf{v} = v_\parallel\mathbf{b} + \mathbf{v}_\perp$, with

$$\mathbf{v}_\perp = \mathbf{v} - (\mathbf{b}\cdot\mathbf{v})\mathbf{b}, \tag{2.14}$$

and similarly for the **E**-field. From the equations of motion, Eq. (2.3), we then find

$$\dot{v} = \frac{\mathbf{v}\cdot\dot{\mathbf{v}}}{v} = \frac{q_a}{m_a}\frac{\mathbf{v}\cdot\mathbf{E}}{v} = \frac{q_a}{m_a}E_\parallel\xi + \frac{q_a}{m_a}E_\perp\sqrt{1-\xi^2}\cos\varphi, \tag{2.15}$$

$$\begin{aligned}\dot{\xi} &= \frac{\mathrm{d}}{\mathrm{d}t}\left(\frac{\mathbf{v}\cdot\mathbf{b}}{v}\right) = \frac{\mathbf{v}}{v}\cdot\dot{\mathbf{b}} + \frac{q_a}{m_a}\frac{1}{v}\left(\mathbf{E}\cdot\mathbf{b} - \frac{\mathbf{b}\cdot\mathbf{v}}{v^2}\mathbf{E}\cdot\mathbf{v}\right)\\ &= \frac{\mathbf{v}}{v}\cdot\dot{\mathbf{b}} + \frac{q_a}{m_a}\frac{1-\xi^2}{v}E_\parallel - \frac{q_a}{m_a}E_\perp\xi\sqrt{1-\xi^2}\cos\varphi.\end{aligned} \tag{2.16}$$

Similarly we can evaluate

$$\frac{\mathrm{d}}{\mathrm{d}t}\Big(\cos\varphi\Big) = \frac{\mathrm{d}}{\mathrm{d}t}\left(\frac{\mathbf{E}_\perp}{E_\perp}\right)\cdot\frac{\mathbf{v}_\perp}{v_\perp} + \frac{q_a}{m_a E_\perp v_\perp}\left(E_\perp^2 - \frac{(\mathbf{E}_\perp\cdot\mathbf{v}_\perp)^2}{v_\perp^2} + \mathbf{E}_\perp\cdot(\mathbf{v}\times\mathbf{B})\right), \tag{2.17}$$

so that

$$\dot{\varphi} = -\frac{\mathrm{d}}{\mathrm{d}t}\left(\frac{\mathbf{E}_\perp}{E_\perp}\right)\cdot\frac{\mathbf{v}_\perp}{\sin\varphi v_\perp} - \frac{q_a E_\perp}{m_a v_\perp}\sin\varphi - \frac{q_a B}{m_a}. \tag{2.18}$$

We will now further assume that we are considering magnetized plasmas, by which we mean that the time-scale of gyromotion, characterized by the gyrofrequency

$$\Omega = \frac{q_a B}{m_a}, \tag{2.19}$$

is much shorter ($1/\Omega \sim 10\,\mathrm{ns}$ for a hydrogen ion at 1 Tesla) than the collisional time-scale τ_c (defined later in Eq. (2.74)) and the time-scale of acceleration by the electric field $\tau_e = m_a v_{Ta}/|q_a E|$ (in our applications of the same order of magnitude as the collisional time-scale). This separation of time-scales allows us to perturbatively solve the kinetic equation by introducing the small ordering parameter

$$\varepsilon = \frac{1}{\Omega\tau_c} \ll 1 \tag{2.20}$$

and writing $f_a = f_{a0} + \varepsilon f_{a1} + \mathcal{O}(\varepsilon^2)$. To order $\mathcal{O}(\varepsilon^{-1})$, the kinetic equation reads

$$\frac{\partial f_{a0}}{\partial\varphi} = 0, \tag{2.21}$$

meaning that the distribution does not depend on the gyroangle to lowest order, and we have

$$f_{a0} = f_{a0}(v,\xi,t). \tag{2.22}$$

To order $\mathcal{O}(\varepsilon^0)$, the equation then reads

$$\frac{\partial f_{a0}}{\partial t} + \dot{v}\frac{\partial f_{a0}}{\partial v} + \dot{\xi}\frac{\partial f_{a0}}{\partial\xi} - \frac{1}{\tau_c}\frac{\partial f_{a1}}{\partial\varphi} = C_a\{f_{a0}\}, \tag{2.23}$$

mixing f_{a0} and f_{a1}. However, we may average the kinetic equation over φ by applying the operation $\frac{1}{2\pi}\int_0^{2\pi}\mathrm{d}\varphi$ on both sides. Performing this gyroaverage, we obtain

$$\frac{1}{2\pi}\int_0^{2\pi}\mathrm{d}\varphi\,\dot{v} = \frac{q_a}{m_a}E_\parallel\xi, \tag{2.24}$$

$$\frac{1}{2\pi}\int_0^{2\pi}\mathrm{d}\varphi\,\dot{\xi} = \frac{q_a}{m_a}\frac{1-\xi^2}{v}E_\parallel - \frac{v_\perp^2}{2v}\,\mathbf{b}\cdot\nabla\ln B, \tag{2.25}$$

$$\frac{1}{2\pi}\int_0^{2\pi}\mathrm{d}\varphi\,\frac{\partial f_{a1}}{\partial\varphi} \equiv 0, \tag{2.26}$$

where we assumed only that f_{a1} must be single-valued in φ. In the expression for the averaged $\dot{\xi}$, the final term is related to the spatial non-homogeneity of the system and is of order $v\,\mathbf{b}\cdot\nabla\ln B \sim v_T/L$, negligible compared to collisional frequency by the same argument with which we neglected parallel transport.

The gyro-averaged kinetic equation then takes the form

$$\frac{\partial f_{a0}}{\partial t} + \frac{q_a}{m_a}E_\parallel\left(\xi\frac{\partial}{\partial v} + \frac{1-\xi^2}{v}\frac{\partial}{\partial\xi}\right)f_{a0} = \bar{C}_a\{f_{a0}\}, \tag{2.27}$$

where $\bar{C}_a$ denotes the gyro-averaged collision operator. This is the form of the kinetic equation used in the paper by Furth and Rutherford in their investigation of the runaway ion distribution [15]. Since this is a closed equation for f_{a0} and we will not consider the higher order term f_{a1}, we may drop the index 0 without ambiguity.

2.2 The Fokker-Planck equation

As the Coulomb interaction in plasmas is long ranged, as opposed to the "billiard ball" collisions used to model ordinary gases, we may use the so-called Fokker-Planck approximation of the collision operator. It can be shown that the cumulative contribution from many small-angle collisions dominate the contributions from large-angle collisions to the collision operator by a factor of order

$$\ln \Lambda = \ln \frac{1}{\theta_{\min}} = \ln \frac{2\pi\varepsilon_0 T \lambda_D}{e^2} = \ln \left[\frac{2\pi}{\sqrt{n}} \left(\frac{\varepsilon_0 T}{e^2} \right)^{3/2} \right], \tag{2.28}$$

where $\theta_{\min}$ is the scattering angle of a particle passing at the Debye length from a charge. $\ln \Lambda$ is called the Coulomb logarithm and is typically of order 15-20 in fusion plasmas [23].

This means that, to good approximation, we need only account for those collisions which only marginally change the momentum of the incident particles. Explicitly, we can check that a typical angular deflection of the incident particles in the center of mass frame, assuming a characteristic impact parameter $\rho = n^{-1/3}$, corresponds to

$$\Delta\theta = \frac{e^2 n^{1/3}}{4\pi\varepsilon_0 T} \sim 10^{-6} \tag{2.29}$$

in fusion plasmas.

Therefore we assume that the collisional dynamics are such that, as a charged particle moves through the plasma and interacts with the background particles, it will perform a near-continuous motion through phase space as it undergoes many small-angle collisions. Since the interactions take place within the Debye sphere and are considered point-wise, and the distribution is locally conserved in velocity space due to the characteristic behaviour of the Coulomb interactions in a plasma described above, we can write the collision operator as

$$C_a = \frac{\partial}{\partial \mathbf{v}} \cdot \mathbf{S}, \tag{2.30}$$

where $\mathbf{S}$ is the particle flux in velocity space induced by collisions. Since collisions change the velocities by finite but small amounts compared to the variation of f_a, the flux at some phase space point $\mathbf{v}$ will depend on the value of the distribution at that coordinate and those nearby. This suggests that to leading order the flux can be represented by the form

$$S_i = \frac{A_i(\mathbf{v})}{m_a} f_a + \frac{\partial}{\partial v_j} \Big[D_{ij}(\mathbf{v}) f_a \Big], \tag{2.31}$$

which is the Fokker-Planck form of the collision operator, essentially taking the form of a Taylor expansion of the full collison operator. We have factorized m_a for $\mathbf{A}$ to have the dimension of force by convention. This being of the form of a differential operator acting on f_a, it is considerably easier to work with than the full collision operator, which is an integral operator coupling the value of the distribution function at all velocities, since it also accounts for large-angle collisions. Such a description would require one to keep an infinite set of terms in the 'Taylor expansion' of $\mathbf{S}$ [23].

By comparing with the kinetic equation, Eq. (2.7), it can be seen that the coefficient $\mathbf{A}$ appears in the same form as the electromagnetic Lorentz force. Because of this, $\mathbf{A}$ can be interpreted as a (velocity-dependent) collisional friction force acting on the particles in the plasma. By neglecting all forces in the kinetic equation, one obtains a non-isotropic

diffusion equation in velocity space with diffusion tensor D_{ij}, allowing for the interpretation of the corresponding term in the kinetic equation as associated with collisional diffusion. This is not unexpected, since a particle in a plasma will undergo many collisions which randomly alter the momentum by small amounts, giving rise to a diffusive random-walk like behavior.

2.2.1 Properties of the collision operator

An alternative and often convenient form of the Fokker-Planck collision operator in Eq. (2.31) is given by

$$C_{ab}\{f_a, f_b\} = L_{ab}\frac{\partial}{\partial v_i}\left(\frac{m_a}{m_b}\frac{\partial \varphi_b}{\partial v_i}f_a - \frac{\partial^2 \psi_b}{\partial v_i \partial v_j}\frac{\partial f_a}{\partial v_j}\right), \tag{2.32}$$

$$L_{ab} = \ln\Lambda\left(\frac{q_a q_b}{m_a \varepsilon_0}\right)^2. \tag{2.33}$$

The coefficient L_{ab} is characteristic for Coulomb interactions, explicitly showing the factor $\ln\Lambda$ associated with small-angle collisions. Written in this form, a careful study of binary collision statistics with the Coulomb interaction – which will not be presented in this thesis but may be found in standard plasma physics literature [16, 23, 24, 31] – yields the following form for the so-called Rosenbluth potentials φ and ψ:

$$\varphi_b = -\frac{1}{4\pi}\int \mathrm{d}^3\mathbf{v}'\,\frac{f_b(\mathbf{v}')}{|\mathbf{v}-\mathbf{v}'|}, \tag{2.34}$$

$$\psi_b = -\frac{1}{8\pi}\int \mathrm{d}^3\mathbf{v}'\,|\mathbf{v}-\mathbf{v}'| f_b(\mathbf{v}'). \tag{2.35}$$

Note that the Rosenbluth potentials are related by

$$\nabla^2\varphi_b = f_b, \tag{2.36}$$

$$\nabla^2\psi_b = \varphi_b. \tag{2.37}$$

Comparing the expressions, we may identify the coefficient of friction

$$A_i = \sum_b L_{ab} m_a \left(1 + \frac{m_a}{m_b}\right)\frac{\partial \varphi_b}{\partial v_i}, \tag{2.38}$$

and the diffusion tensor

$$D_{ij} = -\sum_b L_{ab}\frac{\partial^2 \psi_b}{\partial v_i \partial v_j}. \tag{2.39}$$

Properties of the Fokker-Planck collision operator include particle conservation of all species,

$$\int \mathrm{d}^3\mathbf{v}\, C_{ab}(f_a, f_b) \equiv 0, \tag{2.40}$$

which follows immediatly from the divergence form Eq. (2.30) of the collision operator. Conservation of total momentum and energy between the interacting species is ensured by the identities

$$\mathbf{R}_{ab} \equiv \int \mathrm{d}^3\mathbf{v}\, m_a \mathbf{v} C_{ab}\{f_a, f_b\} = -\int \mathrm{d}^3\mathbf{v}\, m_b \mathbf{v} C_{ba}\{f_b, f_a\} \equiv -\mathbf{R}_{ba}, \tag{2.41}$$

where $\mathbf{R}_{ab}$ is the total force on species a due to collisions with species b, and

$$\int \mathrm{d}^3\mathbf{v}\,\frac{m_a v^2}{2} C_{ab}(f_a, f_b) = -\int \mathrm{d}^3\mathbf{v}\,\frac{m_b v^2}{2} C_{ba}(f_b, f_a). \tag{2.42}$$

For self-collisions these reduce to

$$0 \equiv \int \mathrm{d}^3\mathbf{v}\,\mathbf{v} C_{aa}\{f_a\} = \int \mathrm{d}^3\mathbf{v}\,v^2 C_{aa}\{f_a\}. \tag{2.43}$$

It can be shown that the collision operator also satisfies the so-called H-theorem: the property that collisions increase the entropy of the system, defined as $S = \int \mathrm{d}^3\mathbf{v}\, f_a(1 - \ln f_a)$ [24]. The entropy is maximized by distributions of the form

$$f_M(\mathbf{v}) = n\left(\frac{m}{2\pi T}\right)^{3/2} \exp\left(-\frac{m(\mathbf{v}-\mathbf{V})^2}{2T}\right), \tag{2.44}$$

known as a Maxwellian distribution, and the collision operator between two such distributions vanish when they are at the same temperature T and flow velocity $\mathbf{V}$.

From Eq. (2.32) together with (2.34) and (2.35) it is clear that the collision operator is a bilinear operator, satisfying

$$C_{ab}\{f_{a1} + f_{a2}, f_{b1} + f_{b2}\} = C_{ab}\{f_{a1}, f_{b1}\} + C_{ab}\{f_{a1}, f_{b2}\} + C_{ab}\{f_{a2}, f_{b1}\} + C_{ab}\{f_{a2}, f_{b2}\}, \tag{2.45}$$

with the implication that the kinetic equation is non-linear, since for self-collisions

$$C_{aa}\{f_{a1} + f_{a2}\} = C_{aa}\{f_{a1}\} + C_{aa}\{f_{a2}\} + C_{aa}\{f_{a1}, f_{a2}\} + C_{aa}\{f_{a2}, f_{a1}\}. \tag{2.46}$$

If we consider only small departures from some thermal equilibrium, we can write

$$f_b = f_{b0} + f_{b1}, \tag{2.47}$$

where f_{b0} are Maxwellian distributions with common temperatures and drift velocities, and f_{b1} are the departures from equilibrium. We may then approximate

$$C_{ab}\{f_a, f_b\} = C_{ab}\{f_a, f_{b0}\} + C_{ab}\{f_{a0}, f_b\}, \tag{2.48}$$

where terms quadratic in f_1 are neglected and the property $C_{ab}\{f_{a0}, f_{b0}\} \equiv 0$ is used. This is the linearized collision operator. The first term accounts for collisions between the perturbed distribution f_a with background particles of species b and is called the test-particle operator, while the second term accounts for the effect on the background particles of a due to the perturbed distribution f_b and is called the field-particle operator.

It can be shown that the linearized collision operator vanishes for distributions on the form

$$f = (\alpha + \boldsymbol{\beta}\cdot\mathbf{v} + \gamma v^2) e^{-v^2/2mT}, \tag{2.49}$$

the set of perturbed Maxwellians. This illustrates how the linearized collision operator fails to correctly describe the dynamics of strongly perturbed distributions, as could be expected from neglecting the term quadratic in the perturbation. The linearized collision operator, like the full one, satisfies conservation of particle number, momentum and energy. The test-particle and field-particle operators alone satisfy only conservation of particle number.

2.2.2 Test-particle collision operator

The test-particle collision operator can be evaluated explicitly. We have to calculate the Rosenbluth potentials φ_b and ψ_b for a Maxwellian distribution, which can be done by solving the system of equations

$$\nabla^2\varphi_b = \frac{n_b}{\pi^{3/2}v_{Tb}^3}\exp\left(-\frac{(\mathbf{v}-\mathbf{V}_b)^2}{v_{Tb}^2}\right), \tag{2.50}$$

$$\nabla^2\psi_b = \varphi_b, \tag{2.51}$$

where we introduced the thermal velocity $v_{Tb} = \sqrt{2T_b/m_b}$. In a frame where $\mathbf{V}_b$ vanishes, the system is spherically symmetric and the potentials can be functions only of $v = |\mathbf{v}|$. This considerably simplifies the Fokker-Planck operator, and we may note that, writing $\partial\varphi_b(v)/\partial v = \varphi_b'$,

$$\frac{\partial}{\partial v_i}\left(\frac{\partial\varphi_b}{\partial v_i}f_a\right) = \frac{\partial}{\partial v_i}\left(\frac{v_i}{v}\varphi_b' f_a\right) = \frac{2}{v}\varphi_b' f_a + \frac{1}{v}v_i\frac{\partial}{\partial v_i}\left(\varphi_b' f_a\right). \tag{2.52}$$

With $v_i\partial/\partial v_i \equiv v\partial/\partial v$ we can identify that

$$\frac{\partial}{\partial v_i}\left(\frac{\partial\varphi_b}{\partial v_i}f_a\right) = \frac{1}{v^2}\frac{\partial}{\partial v}\left(v^2\varphi_b' f_a\right). \tag{2.53}$$

We also have

$$\frac{\partial^2\psi_b}{\partial v_i\partial v_j} = \frac{\partial}{\partial v_j}\left(\frac{v_i}{v}\psi_b'\right) = \frac{1}{v}\left(\delta_{ij} - \frac{v_iv_j}{v^2}\right)\psi_b' + \frac{v_iv_j}{v^2}\psi_b''. \tag{2.54}$$

Here, $(\delta_{ij} - v_iv_j/v^2)$ is effectively a projection operator, projecting vectors on the subspace perpendicular to v_i. This means that its contraction with v_i or v_j vanishes, which will greatly simplify the expressions. However, the second term above appears in the collision operator as

$$-\frac{\partial}{\partial v_i}\left(\frac{v_iv_j}{v^2}\psi_b''\frac{\partial f_a}{\partial v_j}\right) = -\frac{\partial}{\partial v_i}\left(\psi_b''\frac{v_i}{v}\frac{\partial f_a}{\partial v}\right) = -\frac{1}{v^2}\frac{\partial}{\partial v}\left(v^2\psi_b''\frac{\partial f_a}{\partial v}\right), \tag{2.55}$$

following from a calculation analogous to the one leading to Eq. (2.53). The final term is

$$\begin{aligned}-\frac{\partial}{\partial v_i}\left(\frac{1}{v}\left(\delta_{ij} - \frac{v_iv_j}{v^2}\right)\psi_b'\frac{\partial f_a}{\partial v_j}\right) &= \frac{2}{v^2}\psi_b'\frac{\partial f_a}{\partial v} - \frac{\psi_b'}{v}\left(\delta_{ij} - \frac{v_iv_j}{v^2}\right)\frac{\partial^2 f_a}{\partial v_i\partial v_j}\\ &= -\frac{\psi_b'}{v}\left(\delta_{ij} - \frac{v_iv_j}{v^2}\right)\frac{\partial^2 f_a}{\partial\tilde{v}_i\partial\tilde{v}_j},\end{aligned} \tag{2.56}$$

where $\tilde{v}_i$ denote only the angular coordinates, in the sense that we have written

$$\frac{\partial}{\partial v_i} = \frac{v_i}{v}\frac{\partial}{\partial v} + \frac{\partial}{\partial\tilde{v}_i}. \tag{2.57}$$

On these derivatives, the projection operator acts as the identity (this can be confirmed in a straight-forward but slightly tedious manner by introducing a spherical coordinate system), and the term reduces to

$$-\frac{\partial}{\partial v_i}\left(\frac{1}{v}\left(\delta_{ij} - \frac{v_iv_j}{v^2}\right)\psi_b'\frac{\partial f_a}{\partial v_j}\right) = -\frac{\psi_b'}{v}\nabla_\Omega^2 f_a, \tag{2.58}$$

proportional to the angular part ∇^2_Ω of the Laplace operator. The only dependence on the gyroangle φ in the Fokker-Planck operator is due to the contribution from this final term, which identically vanishes when gyroaveraged since it can be written as a divergence.

Putting it all together, using the expression for the Laplace operator in spherical coordinates, the gyro-averaged Fokker-Planck operator for collisions with a spherically symmetric distribution takes the form

$$\bar{C}_{ab}\{f_a, f_b\} = -L_{ab}\frac{\psi_b'}{v^3}\frac{\partial}{\partial\xi}\left[(1-\xi^2)\frac{\partial \bar{f}_a}{\partial\xi}\right] + L_{ab}\frac{1}{v^2}\frac{\partial}{\partial v}\left(\frac{m_a}{m_b}v^2\varphi_b'\bar{f}_a - v^2\psi_b''\frac{\partial \bar{f}_a}{\partial v}\right). \quad (2.59)$$

We will now drop the superfluous bars on gyroaveraged quantities as no further quantities will depend on gyroangle unless explicitly stated.

From the formula for the divergence in spherical coordinates,

$$\frac{\partial}{\partial \mathbf{v}}\cdot\mathbf{S} = \frac{1}{v^2}\frac{\partial}{\partial v}\Big(v^2 S_v\Big) + \frac{1}{v}\frac{\partial}{\partial\xi}\Big(\sqrt{1-\xi^2}S_\xi\Big), \quad (2.60)$$

we see that we can write the collision operator in divergence (flux) form, with fluxes

$$S_v = L_{ab}\frac{m_a}{m_b}\varphi_b' f_a - L_{ab}\psi_b''\frac{\partial f_a}{\partial v}, \quad (2.61)$$

$$S_\xi = -L_{ab}\frac{\psi_b'}{2v^2}\sqrt{1-\xi^2}\frac{\partial f_a}{\partial\xi}. \quad (2.62)$$

It is now appropriate to evaluate the potentials φ_b', ψ_b' and ψ_b'' for the case of a Maxwellian distribution. The equation for φ_b,

$$\frac{1}{v^2}\frac{\partial}{\partial v}\Big(v^2\varphi_b'\Big) = \frac{n_b}{\pi^{3/2}v_{Tb}^3}\exp\left(\frac{v^2}{v_{Tb}^2}\right), \quad (2.63)$$

can be integrated to yield

$$\varphi_b'(v) = \frac{n_b}{\pi^{3/2}}\frac{1}{v^2}\int_0^{v/v_{Tb}} \mathrm{d}x\, x^2 e^{-x^2} = \frac{n_b}{2\pi v_{Tb}^2}G(x_b), \quad (2.64)$$

where

$$G(x) = \frac{\phi(x) - x\phi'(x)}{2x^2}, \quad (2.65)$$

$$\phi(x) = \frac{2}{\sqrt{\pi}}\int_0^x \mathrm{d}s\, e^{-s^2}, \quad (2.66)$$

$$x_b = v/v_{Tb}. \quad (2.67)$$

Here, $G(x)$ is the Chandrasekhar function and $\phi(x)$ the error function, defined in section 1.3.2, Eq. (1.4). Note that we can write

$$G(x) = -\frac{\mathrm{d}}{\mathrm{d}x}\left(\frac{\phi(x)}{2x}\right), \quad (2.68)$$

allowing us to identify

$$\varphi_b(v) = -\frac{n_b}{4\pi v_{Tb}}\frac{\phi(x_b)}{x_b}. \quad (2.69)$$

The equation for ψ_b can then similarly be integrated,

$$\psi_b' = \frac{1}{v^2}\int \mathrm{d}v\, v^2\varphi_b = -\frac{n_b}{4\pi}\frac{1}{x_b^2}\int_0^{x_b}\mathrm{d}x\, x\phi(x) = -\frac{n_b}{4\pi}\frac{1}{x_b^2}\left(\left[\frac{x^2}{2}\phi(x)\right]_0^{x_b} - \frac{1}{\sqrt{\pi}}\int_0^{x_b}\mathrm{d}x\, x^2 e^{-x^2}\right)$$
$$= -\frac{n_b}{8\pi}\Big(\phi(x_b) - G(x_b)\Big). \tag{2.70}$$

Differentiating finally yields

$$\psi_b'' = -\frac{n_b}{4\pi v_{Tb}}\frac{G(x_b)}{x_b}. \tag{2.71}$$

Putting it all together, the test-particle collision operator takes the form

$$C_{ab}\{f_a, f_{b0}\} = \frac{1}{\tau_{ab}}\Bigg\{\frac{\phi(x_b) - G(x_b)}{2x^3}\frac{\partial}{\partial\xi}\left[(1-\xi^2)\frac{\partial f_a}{\partial\xi}\right]$$
$$+ \frac{1}{x^2}\frac{\partial}{\partial x}\left(2\frac{T_a}{T_b}x^2 G(x_b) f_a + xG(x_b)\frac{\partial f_a}{\partial x}\right)\Bigg\}, \tag{2.72}$$

$$\frac{1}{\tau_{ab}} = \ln\Lambda\frac{n_b}{4\pi}\left(\frac{q_a q_b}{m_a\varepsilon_0}\right)^2\frac{1}{v_{Ta}^3}, \tag{2.73}$$

$$x = v/v_{Ta}, \tag{2.74}$$

$$T_j = \frac{m_j v_{Tj}^2}{2}, \tag{2.75}$$

where we have introduced the collision time τ_{ab}, defining a characteristic time-scale for collisions between two species.

The friction and diffusion coefficients in Eqs. (2.38) and (2.39) are given by

$$A_{ab,v} = \frac{v_i}{v}A_{ab,i} = L_{ab}m_a\left(1+\frac{m_a}{m_b}\right)\varphi_b' = 2\frac{m_a v_{Ta}}{\tau_{ab}}\frac{T_a}{T_b}\left(1+\frac{m_b}{m_a}\right)G(x_b), \tag{2.76}$$

$$D_{ab,vv} = \frac{v_i v_j}{v^2}D_{ab,ij} = -L_{ab}\psi_b'' = \frac{v_{Ta}^2}{\tau_{ab}}\frac{G(x_b)}{x}, \tag{2.77}$$

$$D_{ab,\xi\xi} = \frac{1}{v^2}\left(\delta_{3i} - \frac{v_i}{v}\xi\right)\left(\delta_{3j} - \frac{v_j}{v}\xi\right)D_{ab,ij} = -L_{ab}\frac{1}{v^3}\left(\delta_{3j} - \frac{v_j}{v}\xi\right)^2\psi_b'$$
$$= -L_{ab}\frac{1-\xi^2}{v^3}\psi_b' = \frac{1}{\tau_{ab}}(1-\xi^2)\frac{\phi(x_b) - G(x_b)}{2x^3}, \tag{2.78}$$

with all other matrix elements vanishing, as is clear from the final form of the collision operator. Note that A only has a radial v-component, meaning that it represents an isotropic slowing-down force.

It is useful to evaluate the momentum and energy moments of the collision operator. They are given by

$$\mathbf{R}_{ab} = \int \mathrm{d}^3\mathbf{v}\, m_a\mathbf{v}C_{ab}(f_a, f_b) = \int \mathrm{d}^3\mathbf{v}\,\mathbf{v}\frac{\partial}{\partial\mathbf{v}}\cdot\left[\mathbf{A}_{ab}f_a + m_a\frac{\partial}{\partial\mathbf{v}}\cdot\Big(D_{ab}f_a\Big)\right]$$
$$= -\int \mathrm{d}^3\mathbf{v}\,\mathbf{A}_{ab}f_a, \tag{2.79}$$

$$Q_{ab} = \int \mathrm{d}^3\mathbf{v}\,\frac{m_a v^2}{2}C_{ab}(f_a, f_b) = \int \mathrm{d}^3\mathbf{v}\,\frac{v^2}{2}\frac{\partial}{\partial\mathbf{v}}\cdot\left[\mathbf{A}_{ab}f_a + m_a\frac{\partial}{\partial\mathbf{v}}\cdot\Big(D_{ab}f_a\Big)\right]$$
$$= \int \mathrm{d}^3\mathbf{v}\left[-\mathbf{v}\cdot\mathbf{A}_{ab} + m_a\mathrm{Tr}(D_{ab})\right]f_a, \tag{2.80}$$

a form which is obtained after integrating by parts twice and using the divergence theorem, neglecting the boundary fluxes at infinity. From the definition of the diffusion tensor it is clear that $\mathrm{Tr}(D_{ab}) = -L_{ab}\nabla^2\psi_b = -L_{ab}\varphi_b$.

For the case of the test-particle operator, we obtain

$$\mathbf{R}_{ab,0} = -2\frac{m_a v_{Ta}}{\tau_{ab}}\frac{T_a}{T_b}\left(1+\frac{m_b}{m_a}\right)\int \mathrm{d}^3\mathbf{v}\,\mathbf{v}\frac{G(x_b)}{v}f_a, \tag{2.81}$$

$$Q_{ab,0} = -\frac{m_a v_{Ta}^2}{\tau_{ab}}\int \mathrm{d}^3\mathbf{v}\left[2\frac{T_a}{T_b}\left(1+\frac{m_b}{m_a}\right)xG(x_b) - \frac{\phi(x_b)}{x}\right]f_a, \tag{2.82}$$

for the rate of momentum and energy transfer to a Maxwellian species.

2.3 Kinetic equation for ions

In this section we will demonstrate how an appropriate collision operator for runaway ions can be constructed. We will consider a plasma consisting of an arbitrary set of ion species i with densities n_i, masses m_i, charge number Z_i and temperatures T_i, and an electron population of temperature T_e and density n_e such that the overall plasma is charge neutral: $\sum_i n_i Z_i/n_e = 1$.

Inter-species ion collisions

We will solve for the ion species which is accelerated at the highest rate. Therefore all other ion species will be taken to remain in the equilibrium distributions f_{i0} during the time-intervals considered. Thus, collisions with other ion species are represented by the test-particle operator

$$C_{ai}\{f_a\} = \sum_j C_{aj}\{f_a, f_{j0}\}, \tag{2.83}$$

where the sum is over all other ion species j in the plasma. It is not straight forward to determine a priori whether this assumption is valid, but with simulation it can be investigated whether the other ion species remain near the equilibrium state during the relevant time ranges. We further assume that all atoms in the plasma are ionized, so that we do not need to account for collisions with neutrals.

In the presence of an accelerating electric field, momentum and energy will continuously be added to the runaway ion distribution. To study the runaway distribution with the linearized equation, collisions with the other ion species provide an important sink of momentum and energy to ensure that the distribution will stay sufficiently close to its equilibrium state. In the absence of impurities, the entire ion distribution would be uniformly accelerated and the model would break down.

Self-collisions

For self-collisions, we cannot consistently neglect the field-particle operator, since it will be of the same order of magnitude as the test-particle term. However, the field-particle operator accounts for the reaction of the bulk distribution to the evolution of the fast population, and as can be seen from Eq. (2.32) the term will be of magnitude $C \sim f_{a0} \sim \exp(-x^2)$. Therefore the field-particle operator will not significantly affect the dynamics of the fast ions, but it will ensure that energy and momentum is not lost from the distribution in self-collisions. This can affect the rate at which fast ions are produced.

Calculating the Rosenbluth potentials of the runaway distribution is numerically expensive, and we will seek an alternative, faster approach. This is achieved by introducing a so-called model operator, which is a collision operator assumed to take a simple form and constructed to achieve a desired set of properties – for example satisfying the conservation laws, Eqs. (2.40) and (2.43). These techniques are discussed in a paper by Hirshman and Sigmar [32].

We will use an ion self-collision operator on the form

$$C_{aa}\{f_a\} = C_{aa}(f_a, f_{a0}) + C^{(m)}_{aa}(f_{a0}, f_a), \tag{2.84}$$

where $C^{(m)}$ is the model field-particle operator. For the choice of this operator, we will use the form recently developed by Abel *et al.* for linearised problems, which satisfies both the H-theorem mentioned in section 2.2.1 and satisfies momentum conservation and energy conservation, Eq. (2.43). This operator has the gyrophase-dependent form

$$C^{(m)}_{aa}(f_{a0}, f_a) = \frac{1}{\tau_{aa}}\left(w_1(v)\frac{\mathbf{u}\cdot\mathbf{v}}{v_{Ta}} + w_2(v)Q\frac{v^2}{v^2_{Ta}}\right)f_{a0}(v), \tag{2.85}$$

where w_1 and w_2 are functions of v chosen so that the operator will satisfy number conservation, self-adjointness and the H-theorem, and the quantities $\mathbf{u}\{f_a\}$ and $Q\{f_a\}$ are calculated from the runaway distribution f_a in such a way that momentum and energy will be conserved in self-collisions. Note that the first term is odd in $\mathbf{v}$ with the consequence that it will carry momentum but not energy, and vice versa for the second term which is even. Momentum and energy conservation in self-collisions is given by the conditions

$$0 = \mathbf{R}_{aa} = \mathbf{R}_{aa,0} + \frac{m_a}{\tau_{aa}}u_j\int \mathrm{d}^3\mathbf{v}\, w_1(v)v_iv_jf_{a0}(v), \tag{2.86}$$

$$0 = Q_{aa} = Q_{aa,0} + \frac{m_aQ}{2v^2_{Ta}}\int \mathrm{d}^3\mathbf{v}\, w_2(v)v^4f_{a0}(v). \tag{2.87}$$

Using the identity

$$\int \mathrm{d}^3\mathbf{v}\, w_1(v)v_iv_jf_{a0}(v) \equiv \frac{\delta_{ij}}{3}\int \mathrm{d}^3\mathbf{v}\, w_1(v)v^2f_{a0}(v) \tag{2.88}$$

since w_1f_{a0} depends only on v, we obtain

$$\mathbf{u} = -3\frac{\tau_{aa}}{m_a}\frac{\mathbf{R}_{aa,0}}{\int \mathrm{d}^3\mathbf{v}\, w_1(v)v^2f_{a0}}, \tag{2.89}$$

$$Q = -2\frac{\tau_{aa}v^2_{Ta}}{m_a}\frac{Q_{aa,0}}{\int \mathrm{d}^3\mathbf{v}\, w_2(v)v^2f_{a0}}. \tag{2.90}$$

Using a different convention than Abel *et al.* [33], we choose for w_1 and w_2,

$$w_1(v) = 2\nu_s(v) \equiv 8\frac{G(x)}{x}, \tag{2.91}$$

$$w_2(v) = \nu_E(v) \equiv 2\left(4\frac{G(x)}{x} - \frac{\phi(x)}{x^3}\right). \tag{2.92}$$

With these definitions, Eqs. (2.81) and (2.82) for $R_{ab,0}$ and $Q_{ab,0}$ take the form

$$\mathbf{R}_{aa,0} = -\frac{1}{\tau_{aa}}\int \mathrm{d}^3\mathbf{v}\, m_a\mathbf{v}\nu_s(v)f_a, \tag{2.93}$$

$$Q_{aa,0} = -\frac{1}{\tau_{aa}}\int \mathrm{d}^3\mathbf{v}\, \frac{m_av^2}{2}\nu_E(v)f_a, \tag{2.94}$$

and we obtain

$$\mathbf{u} = \frac{3}{2} v_{Ta} \frac{\int \mathrm{d}^3\mathbf{v}\, \mathbf{v} \nu_s(v) f_a}{\int \mathrm{d}^3\mathbf{v}\, v^2 \nu_s(v) f_{a0}}, \tag{2.95}$$

$$Q = v_{Ta}^2 \frac{\int \mathrm{d}^3\mathbf{v}\, v^2 \nu_E(v) f_a}{\int \mathrm{d}^3\mathbf{v} v^4 \nu_E(v) f_{a0}}. \tag{2.96}$$

This particular choice of w_1 and w_2 ensures that the operator satisfies number conservation, self-adjointness and non-negative entropy production (properties it shares with the full and linearized collision operators), and that it vanishes when f_a is a perturbed Maxwellian of the form $(\alpha + \boldsymbol{\beta} \cdot \mathbf{v} + \gamma v^2) f_{a0}$.

Since f_a is independent of gyro-angle, $\mathbf{u}$ will be directed in the parallel direction by symmetry. Then, the effect of gyro-averaging the model operator is the reduction of $\mathbf{u} \cdot \mathbf{v}$ to $u_\parallel v_\parallel = u_\parallel v \xi$. The averaged model operator then takes the form

$$\bar{C}_{aa}^{(m)}(f_{a0}, f_a) = \frac{1}{\tau_{aa}} \left(w_1(v) \frac{v}{v_{Ta}} u_\parallel \xi + w_2(v) Q \frac{v^2}{v_{Ta}^2} \right) f_{a0}(v). \tag{2.97}$$

Ion-electron collisions

Under the influence of a small static electric field, reorder is quickly reached in the plasma where the electron distribution is perturbed in such a way that the friction against ions cancels exactly the force from the driving electric field. In the case of a pure plasma with only one ion species, the reaction force from the electrons on the ions also cancels the electric force acting on the ions. However, the reaction force on the ions is sensitive to ion charge, and in the presence of multiple ion species (or magnetic geometry effects, considered by Helander [19] but neglected here) the cancellation will not be complete. Indeed, under certain conditions the friction against electrons can yield a larger accelerating force than that originally due to the electric field. Below we will derive an approximate form of the ion-electron collision operator which demonstrates this behavior.

We will consider the electron distribution perturbed from its equilibrium as discussed at the beginning of this section by an applied electric field, $f_e = f_{e0} + f_{e1}$, where f_{e0} is a Maxwellian with flow velocity the same as that of the ion distribution, and f_{e1} the perturbation from that state. We will thus get a contribution to the ion-electron collision operator of $C_{ae}(f_a, f_{e0})$ – the already familiar test-particle operator. To evaluate the contribution from f_{e1}, we may note from the Fokker-Planck collision operator, Eq. (2.32), that if we only keep the leading term in the large mass ratio $m_a/m_e \gg 1$, it reduces to

$$C_{ae}\{f_a, f_{e1}\} = L_{ae} \frac{m_a}{m_e} \frac{\partial}{\partial \mathbf{v}} \cdot \left(\frac{\partial \varphi_{e1}}{\partial \mathbf{v}} f_a \right). \tag{2.98}$$

We can further use the fact that f_e varies on velocity scales much larger than the ion thermal velocity $v_{Te} \gg v_{Ta}$, and that the perturbed electron distribution f_{e1} due to an electric field (a solution to the so-called Spitzer problem) typically vanishes at zero velocity, with the consequence that it is everywhere valid to expand

$$\varphi_{e1} = -\frac{1}{4\pi} \int \mathrm{d}^3\mathbf{v}' \, \frac{f_{e1}(\mathbf{v}')}{|\mathbf{v} - \mathbf{v}'|} \approx -\frac{1}{4\pi} \int \mathrm{d}^3\mathbf{v}' \, \frac{f_{e1}(\mathbf{v}')}{v'} \left(1 + \frac{\mathbf{v} \cdot \mathbf{v}'}{v'^2} \right). \tag{2.99}$$

Then, to lowest non-vanishing order in $v/v' \sim v_{Ta}/v_{Te} \sim \sqrt{m_e/m_a}$, we obtain

$$\frac{\partial \varphi_{e1}}{\partial \mathbf{v}} \approx -\frac{1}{4\pi} \int \mathrm{d}^3\mathbf{v}' \, \frac{\mathbf{v}'}{v'^3} f_{e1}(\mathbf{v}'). \tag{2.100}$$

We will now show that this corresponds to the electron-ion friction, under the assumption of negligible momentum transfer between the ion distribution and f_{e0}. We showed in Eq. (2.79) that the electron-ion friction force is given by (neglecting the term of order m_e/m_i)

$$\mathbf{R}_{ei} = -L_{ei} m_e \int \mathrm{d}^3\mathbf{v}\, \frac{\partial \varphi_i}{\partial \mathbf{v}} f_e. \tag{2.101}$$

With an analogous argument to that used for Eq. (2.99), we can calculate the potential φ_i for electron-ion collisions,

$$\varphi_i = -\frac{1}{4\pi}\int \mathrm{d}^3\mathbf{v}'\, \frac{f_i(\mathbf{v}')}{|\mathbf{v}-\mathbf{v}'|} \approx -\frac{1}{4\pi}\int \mathrm{d}^3\mathbf{v}'\, \frac{f_i(\mathbf{v}')}{v} = -\frac{n_i}{4\pi v}, \tag{2.102}$$

so that

$$\mathbf{R}_{ei} = -\frac{n_i L_{ei} m_e}{4\pi}\int \mathrm{d}^3\mathbf{v}'\, \frac{\mathbf{v}'}{v'^3} f_e = -\frac{n_i Z_i^2}{n_e}\mathbf{R}_0, \tag{2.103}$$

where $\mathbf{R}_0$ is independent of ion species. From the condition that the total electron-ion friction cancels the electric force acting on the electrons, we get

$$-n_e e\mathbf{E} = -\sum_i \frac{n_i Z_i^2}{n_e}\mathbf{R}_0 \equiv -Z_{\mathrm{eff}}\mathbf{R}_0, \tag{2.104}$$

where we have introduced the effective charge $Z_{\mathrm{eff}} = \sum_i n_i Z_i^2/n_e$, so that

$$\mathbf{R}_0 = \frac{1}{4\pi}\frac{m_e v_{Te}^3}{\tau_{ee}}\int \mathrm{d}^3\mathbf{v}'\, \frac{\mathbf{v}'}{v'^3} f_e \equiv \frac{n_e e\mathbf{E}}{Z_{\mathrm{eff}}}. \tag{2.105}$$

Combining the above expressions, we finally conclude that the ion-electron field-particle operator takes the form

$$C_{ae}\{f_a, f_{e1}\} = L_{ae}\frac{m_a}{m_e}\frac{\partial}{\partial \mathbf{v}}\cdot\left(\frac{\partial \varphi_{e1}}{\partial \mathbf{v}} f_a\right) = \frac{Z_a}{Z_{\mathrm{eff}}}\frac{q_a}{m_a}\mathbf{E}\cdot\frac{\partial f_a}{\partial \mathbf{v}}. \tag{2.106}$$

The term appears in the kinetic equation with exactly the same form as the electric field-term. Thus we can compactly account for this by replacing in the ion kinetic equation E by the effective electric field

$$E^* = \left(1 - \frac{Z_a}{Z_{\mathrm{eff}}}\right) E. \tag{2.107}$$

It is now clear that for a pure plasma of one ion species, $Z_a = Z_{\mathrm{eff}}$ and the ions will experience no net accelerating field due to its cancellation against electron friction. In the presence of impurities so that $Z_{\mathrm{eff}} > Z_a$, there will be a finite effective electric field and ions can in principle overcome collisional friction and be accelerated as runaways until bulk electron friction eventually stops the acceleration. For an impurity of charge $Z > Z_{\mathrm{eff}}$, electron friction will drag it against the electric field and it can be accelerated in the direction opposite to the one expected intuitively.

We have now accounted for all collisions in the plasma, and can finally write down the kinetic equation that governs the time-evolution of the ion distribution. With the sum b running over all particle species in the plasma, it takes the form

$$\frac{\partial f_a}{\partial t} + \frac{q_a}{m_a}E_\parallel^*\left(\xi\frac{\partial}{\partial v} + \frac{1-\xi^2}{v}\frac{\partial}{\partial \xi}\right) f_a = \frac{1}{\tau_{ae}}\sum_b \frac{n_b Z_b^2}{n_e}\left[\frac{\phi(x_b) - G(x_b)}{2x^3}\frac{\partial}{\partial \xi}\left[(1-\xi^2)\frac{\partial f_a}{\partial \xi}\right]\right.$$
$$\left. + \frac{1}{x^2}\frac{\partial}{\partial x}\left(2\frac{T_a}{T_b}x^2 G(x_b) f_a + x G(x_b)\frac{\partial f_a}{\partial x}\right)\right] + C_{aa}^{(m)}\{f_a\}. \tag{2.108}$$

2.4 Test-particle friction force

In this section it will be shown how the collisional friction force on a test-particle depends on velocity, determining under which conditions ion runaway is possible and what velocity the runaways can reach.

To begin with we may consider the forces that act on a test-particle in a plasma. In the parallel direction, there will be the accelerating electric field

$$F_E = q_a E^*. \tag{2.109}$$

We can compare this with the collisional friction force. If we assume that we are considering a sufficiently fast particle, such that the self-collision field-particle term (proportional to $\exp(-x^2)$) is negligible, the friction force is given by the test-particle friction

$$F_c = -A_v = -\sum_b A_{ab,v} = -2\frac{m_a v_{Ta}}{\tau_{ae}} \sum_b \frac{n_b Z_b^2}{n_e}\frac{T_a}{T_b}\left(1+\frac{m_b}{m_a}\right) G(x_b) \tag{2.110}$$

$$= -q_a E_D \frac{T_e}{T_a} Z_a \sum_b \frac{n_b Z_b^2}{n_e}\frac{T_a}{T_b}\left(1+\frac{m_b}{m_a}\right) G(x_b), \tag{2.111}$$

where the sum includes all ion species and electrons, and we have introduced the so-called Dreicer field E_D, a characteristic electric field for collisions defined as

$$E_D = 2\frac{m_e v_{Te}}{e\tau_{ee}} = \frac{m_a v_{Ta}}{\tau_{ae}}\frac{T_a}{T_e}\frac{2}{eZ_a^2} = \ln\Lambda \frac{n_e}{4\pi}\frac{e^3}{\varepsilon_0^2 T_e}. \tag{2.112}$$

A runaway ion is characterized by a velocity $v \gg v_{Ta}$ much larger than the thermal ion velocity. However, for the applications we considered this will still be much smaller than the electron thermal velocity, which is of order 100 times larger than the thermal ion velocities. We are thus interested in the velocity range $x_i \ll v/v_{Ta} \ll x_e$, so for runaway ion dynamics we may use the asymptotic forms for the Chandrasekhar function at low velocities (for electron friction) and high velocities (ion friction):

$$G(x_e) \approx \frac{2}{3\sqrt{\pi}} x_e = \frac{2}{3\sqrt{\pi}}\sqrt{\frac{T_a m_e}{T_e m_a}}x, \tag{2.113}$$

$$G(x_i) \approx \frac{1}{2x_i^2} = \frac{T_i m_a}{T_a m_i}\frac{1}{2x^2}. \tag{2.114}$$

These approximations allow us to find a simple analytic estimate for the runaway velocity. The friction force takes the form

$$F_c = -\frac{m_a v_{Ta}}{\tau_{ae}}\left(\frac{Z_{\mathrm{eff}}+\bar{n}}{x^2} + \frac{4}{3\sqrt{\pi}}\left(\frac{T_a}{T_e}\right)^{3/2}\sqrt{\frac{m_e}{m_a}}x\right), \tag{2.115}$$

where we have introduced

$$\bar{n} = \sum_i \frac{n_i Z_i^2}{n_e}\frac{m_a}{m_i}, \tag{2.116}$$

which is near Z_a if $m_a/m_i \approx Z_a/Z_i$ (being the case for fully ionized atoms).

Consider first the minimum value of the magnitude of the collisional friction force; this will determine the minimum electric field which can accelerate a fast test-ion. It is

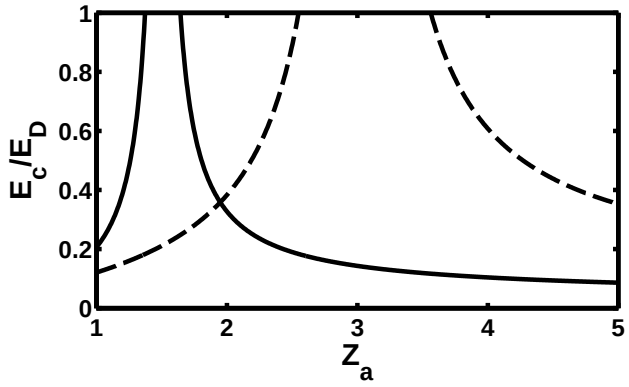

Figure 2.1: Dependence on ion charge of the minimum electric field E_c needed to produce runaways. The solid line shows $Z_{\rm eff} = 1.5$ and the dashed line $Z_{\rm eff} = 3$. Ions are assumed to be fully ionized and satisfying $m_1/m_2 = Z_1/Z_2$.

straight-forward to show that

$$v_{\rm min} = \left(\frac{3\sqrt{\pi}}{2}\frac{m_e}{m_a}(Z_{\rm eff}+\bar{n})\right)^{1/3} v_{Te}, \tag{2.117}$$

$$F_{c,\rm min} \equiv F_c(v_{\rm min}) = -2\frac{m_a v_{Ta}}{\tau_{ae}}\frac{T_a}{T_e}\left(\frac{3}{2\pi}\frac{m_e}{m_a}(Z_{\rm eff}+\bar{n})\right)^{1/3}. \tag{2.118}$$

It follows that the minimum value E_c of the electric field above which a test-ions can be accelerated is given by

$$\frac{E_c}{E_D} = \frac{F_{c,\rm min}}{q_a|1-Z_a/Z_{\rm eff}|E_D} = \frac{Z_a(Z_{\rm eff}+\bar{n})^{1/3}}{|1-Z_a/Z_{\rm eff}|}\left(\frac{3}{2\pi}\frac{m_e}{m_a}\right)^{1/3}. \tag{2.119}$$

We are mainly interested in studying scenarios with electric fields near this value, since this allows a small enough amount of ions – such that they can be considered a small perturbation – to be accelerated. In addition, the derivation of the effective electric field requires the electron distribution to reach a near-equilibrium state where friction against ions cancels the electric field, which is not possible with strong electric fields where the electrons themselves run away.

Figure 2.1 shows the dependence of E_c on ion charge Z_a at different $Z_{\rm eff}$. It is clear from the figure that ions of charge near $Z_{\rm eff}$ will not easily be accelerated, unless the electric fields are very strong. Figure 2.2 shows the electric field $E/E_D = F_c(v)/(q_a E_D|1-Z_a/Z_{\rm eff}|)$ needed to overcome the test-particle collisional friction as function of particle velocity for different plasma compositions. Because of the effective electric field due to electron friction, these diagrams are very sensitive to plasma composition for species with charge near $Z_{\rm eff}$. The figures also highlight the fact that it might not be intuitively obvious which ion species will be accelerated first.

Figure 2.2 illustrates how ion friction dominates at low velocities, while the electron friction peaking at $v = v_{Te}$ dominates at higher velocities. Imagining a horizontal line in the figure representing the accelerating force due to an electric field, one can read off to which velocity ions from each species will be accelerated.

We may now find the critical runaway velocities v_{c1} (threshold velocity above which particles become runaways) and v_{c2} (accumulation point where electron friction cancels

electric field). These are the solutions to the equation $q_a E^* + F_c(v) = 0$. In our approximation, this is a third order polynomial equation, and the resulting answers are not particularily illuminating. Instead we may note that at v_{c1}, ion friction typically dominates, and at v_{c2} electron friction dominates. By neglecting the less important term in the respective cases, one readily obtains

$$v_{c1} = \sqrt{\frac{Z_a E_D}{2E}\frac{T_e}{T_a}\frac{Z_{\text{eff}} + \bar{n}}{|1 - Z_a/Z_{\text{eff}}|}}\, v_{Ta}, \tag{2.120}$$

$$v_{c2} = \frac{3\sqrt{\pi}E}{2E_D}\frac{|1 - Z_a/Z_{\text{eff}}|}{Z_a}\, v_{Te}. \tag{2.121}$$

These generalize the corresponding expressions found by Holman [14]. Note that these formulae are only valid when E is sufficiently larger than E_c, since at E_c ion and electron friction contribute equally, and one can not be neglected for the other. The latter one shows that the runaway ion velocity v_{c2} is approximately proportional to the electric field, and that the velocity is a fraction typically of order $10 - 30\%$ of the electron thermal velocity when $E \sim E_c$. These analytic expressions are intended only as a demonstration of how these quantities scale, and in later computations they will be numerically determined from the full force law.

It is important to point out that the diffusion terms in the kinetic equation have not been accounted for in the derivations of this section, nor the field-particle self collisions, meaning that these results do not provide the full picture. They are meant to give simple estimates that show how the essential quantities scale with the plasma parameters, and to provide a useful physical picture for illustrating the runaway phenomenon. A complete description will be provided only by numerical solution of the kinetic equation.

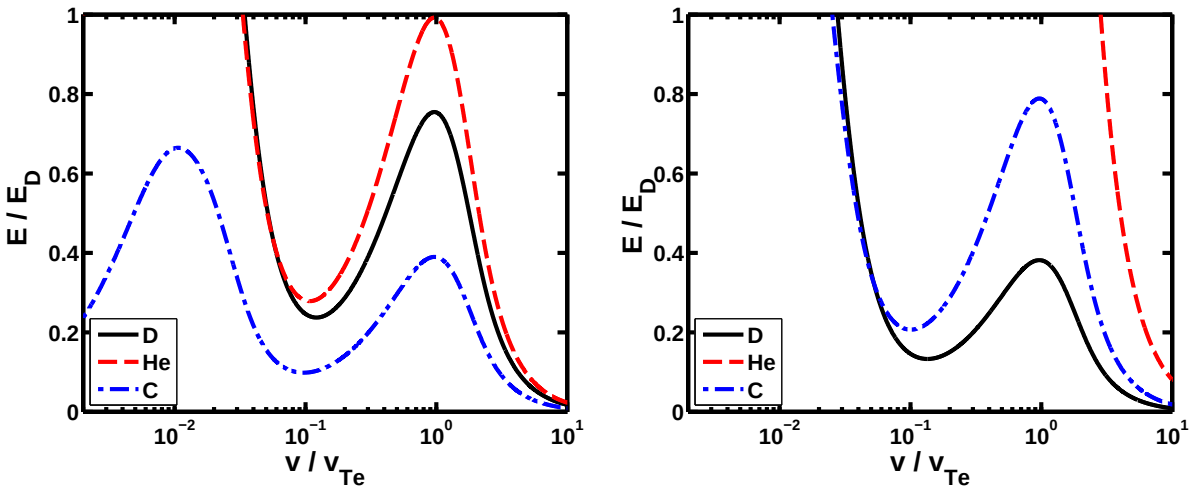

(a) $Z_{\text{eff}} = 1.4$ **(b)** $Z_{\text{eff}} = 2.3$

Figure 2.2: Electric field E needed to overcome collisional friction as a function of velocity for particles of each species in a plasma consisting of deuterium (D), helium (^{4}He) and carbon (C). In both figures, $n_{\text{He}} = 0.1 n_{\text{D}}$. In (a), $n_{\text{C}} = 0.01 n_{\text{D}}$, and in (b) $n_{\text{C}} = 0.06 n_{\text{D}}$. The ion species are fully ionized and at the electron temperature.

Chapter 3

CODION – Numerical implementation

CODION is a numerical tool developed in this work to solve the 2D kinetic equation (Eq. (2.108)) described in the previous chapter. It uses a continuum-spectral discretization scheme based on that used in CODE [22], implemented in MATLAB. CODION allows for explicit time-variation of the electric field and bulk distribution parameters (temperature, density, charge, mass) of each plasma species independently. In this chapter the details of the numerical implementation will be described. We also demonstrate examples of runaway ion behaviour and provide a series of benchmarks, demonstrating energy and momentum conservation properties of the code, comparison to analytic distributions and a cross-comparison with CODE.

3.1 Normalization

CODION solves the kinetic equation Eq. (2.108) with velocity normalized to the thermal velocity $x = v/v_{Ta}$ and time normalized to the ion-electron collision time, a characteristic time-scale for ion runaway,

$$\hat{t} = \frac{t}{\tau_{ae}}. \tag{3.1}$$

Introducing a normalized electric field

$$\hat{E} = \tau_{ae}\frac{q_a E_\parallel^*}{m_a v_{Ta}} = \frac{2}{Z_a}\frac{T_a}{T_e}\frac{E^*}{E_D}, \tag{3.2}$$

the kinetic equation takes the form

$$\frac{\partial f_a}{\partial \hat{t}} + \hat{E}\left(\xi\frac{\partial}{\partial x} + \frac{1-\xi^2}{x}\frac{\partial}{\partial \xi}\right)f_a = \sum_b \frac{n_b Z_b^2}{n_e}\left\{\frac{\phi(x_b) - G(x_b)}{2x^3}\frac{\partial}{\partial \xi}\left[(1-\xi^2)\frac{\partial f_a}{\partial \xi}\right]\right.$$
$$\left. + \frac{1}{x^2}\frac{\partial}{\partial x}\left(2\frac{T_a}{T_b}x^2 G(x_b) f_a + xG(x_b)\frac{\partial f_a}{\partial x}\right)\right\} + \tau_{ae}C_{aa}^{(m)}\{f_a\}, \tag{3.3}$$

where

$$\tau_{ae}C_{aa}^{(m)} = \frac{n_a Z_a^2}{n_e}\left[8G(x)u_\parallel\xi + Q\left(8xG(x) - \frac{\phi(x)}{x}\right)\right]f_{a0}, \tag{3.4}$$

$$u_\parallel = \frac{3}{2}\frac{\int \mathrm{d}^3\mathbf{x}\, G(x)\xi f_a}{\int \mathrm{d}^3\mathbf{x}\, xG(x)f_{a0}}, \tag{3.5}$$

$$Q = \frac{\int \mathrm{d}^3\mathbf{x}\, \left(4xG(x) - \phi(x)/x\right) f_a}{\int \mathrm{d}^3\mathbf{x}\, \left(4x^2G(x) - \phi(x)\right) x f_{a0}}. \tag{3.6}$$

The plasma composition is determined by a set of input vectors $(Z_b, \rho_b, m_b, T_b/T_e)$ of the same but arbitrary length, determining the plasma parameters of each ion species, where $\rho_b = Z_b n_b/n_e$ sums to one to satisfy charge neutrality. In the normalized equation (3.3) which CODION solves, only the ratios of the parameters appear except for charge numbers, with the consequence that arbitrary units may be used for the input.

Since f_a appears linearly in the equation an arbitrary normalization may be chosen for it. This is fixed by the normalization of the initial distribution function, since density is conserved during time-evolution.

3.2 Discretization

The discretization is based on a grid discretization of the velocity coordinate and an expansion in Legendre polynomials of the angular dependence, writing

$$f_a(v,\xi,t) = \sum_{l=0}^{l_{\max}} f_l(v,t)P_l(\xi), \tag{3.7}$$

truncated at some $l_{\max}$ chosen such that f_a is sufficiently well described by the decomposition, and where the Legendre polynomials P_l are normalized to 1 at $\xi = 1$ and therefore satisfy the orthogonality relation

$$\int_{-1}^{1} \mathrm{d}\xi\, P_l(\xi)P_{l'}(\xi) = \frac{2}{2l+1}\delta_{ll'}. \tag{3.8}$$

A linearly independent set of equations is obtained by applying the operator

$$\frac{2L+1}{2}\int_{-1}^{1} \mathrm{d}\xi\, P_L(\xi)... \tag{3.9}$$

to the kinetic equation for each $L = 0, 1, ..., l_{\max}$. Analytic values for each of the terms appearing in the equation are obtained with the identities

$$\frac{2L+1}{2}\int_{-1}^{1} \mathrm{d}\xi\, P_L(\xi)f_a = f_L, \tag{3.10}$$

$$\frac{2L+1}{2}\int_{-1}^{1} \mathrm{d}\xi\, P_L(\xi)\xi f_a = \frac{L+1}{2L+3}f_{L+1} + \frac{L}{2L-1}f_{L-1}, \tag{3.11}$$

$$\frac{2L+1}{2}\int_{-1}^{1} \mathrm{d}\xi\, P_L(\xi)(1-\xi^2)\frac{\partial f_a}{\partial \xi} = \frac{(L+1)(L+2)}{2L+3}f_{L+1} - \frac{(L-1)L}{2L-1}f_{L-1}, \tag{3.12}$$

$$\frac{2L+1}{2}\int_{-1}^{1} \mathrm{d}\xi\, P_L(\xi)\frac{\partial}{\partial \xi}\left[(1-\xi^2)\frac{\partial f_a}{\partial \xi}\right] = -L(L+1)f_L, \tag{3.13}$$

for all L except $L = 0$ for which the f_{L-1}-terms are 0.

The velocity coordinate is discretized on a uniform grid,

$$x_n = n\Delta x \tag{3.14}$$

for $n = 0, 1, ..., x_{\max}/\Delta x$ where Δx and $x_{\max}$ can be chosen arbitrarily. The derivatives appearing in the kinetic equation are discretized with fourth order central finite differences, using

$$\frac{\partial f_L}{\partial x}(x_n) = \frac{1}{12\Delta x}\Big(- f_L(x_{n+2}) + 8f_L(x_{n+1}) - 8f_L(x_{n-1}) + f_L(x_{n-2})\Big), \tag{3.15}$$

$$\frac{\partial^2 f_L}{\partial x^2}(x_n) = \frac{1}{12\Delta x^2}\Big(- f_L(x_{n+2}) + 16f_L(x_{n+1}) - 30f_L(x_n) + 16f_L(x_{n-1}) - f_L(x_{n-2})\Big), \tag{3.16}$$

with a numerical discretization error of order $\mathcal{O}(\Delta x^4)$. At the end points, where $x_{n\pm k}$ would otherwise fall outside the grid, fourth order forward or backward differencing is used instead.

The integral over f appearing in the field-particle self-collision term is discretized with a quadrature of the form

$$\int \mathrm{d}x\, A(x) \approx \sum_n w_n A(x_n). \tag{3.17}$$

For the quadrature weights w_n, we have chosen the so-called alternative extended Simpson's rule [34]:

$$w_n = \frac{\Delta x}{48}\{17, 59, 43, 49, 48, ..., 48, 49, 43, 59, 17\}, \tag{3.18}$$

yielding a quadrature with $\mathcal{O}(\Delta x^4)$ error. An example of how this is used is given by the momentum-restoring self-collision piece in Eq. (3.3), which is computed as

$$u_\parallel \propto \frac{3}{2}\int \mathrm{d}^3\mathbf{x}\, G(x)\xi f_a = 2\pi \sum_n w_n G(x_n) f_1(x_n), \tag{3.19}$$

where the ξ-integral singles out the first Legendre mode of f_a. Unlike the Legendre decomposition which exactly captures the analytic properties of the terms in the equation, the discretization of the velocity derivatives and integrals is approximate, introducing an error (for example to conservation laws) of order $\mathcal{O}(\Delta x^4)$.

The boundary condition at the end-point of the grid is $f_L(x_{\max}) \equiv 0$, for all L. This effectively represents a particle sink at $x_{\max}$, removing particles that reach the maximum resolved velocity. The other "boundary" condition is $f_{l_{\max}}(x) \equiv 0$ for all x. Errors are induced of order $f_L(x_{\max})$ and $f_{l_{\max}}(x)$ due to end-point losses, so the corresponding parameters $x_{\max}$ and $l_{\max}$ have to be chosen sufficiently large so that these functions (depending on L and x respectively) are everywhere negligible for the full duration of a simulation.

Since $P_L(\xi)$ has L nodes between $\xi = -1$ and 1, we effectively cannot resolve details of the distribution function with a width in ξ smaller than $\Delta\xi \lesssim 2/l_{\max}$. The cut-off in L also has the consequence that numerically induced oscillations appear in the solutions, which allows the distribution function to take negative values. However, these typically only occur in regions where the distribution is negligibly small, where the exact values of the distribution function are not of interest for the runaway problem.

Number density, flow velocity and energy density (Eqs. (2.1) and (3.34)) depend only on the first two Legendre modes f_0 and f_1, since they are calculated by integral moments of the distribution with weights proportional to $1 = P_0(\xi)$ and $\xi = P_1(\xi)$. Since the kinetic equation only couples Legendre modes f_l with neighboring ones, $f_{l\pm1}$, the correct conservation properties are exactly satisfied for any $l_{\max} > 2$. Note that errors to conservation are still caused by the discretization of velocity derivatives, which will be discussed further in section 3.4.

With this discretization scheme, the distribution function $f_L(x_n)$ is represented by a vector f_i, where i enumerates the pair (L, n). The discretization of the derivatives and integrals appearing in Eq. (3.3) casts the equation in the form

$$\frac{\partial f_i}{\partial \hat{t}} + \sum_j M_{ij} f_j = 0, \tag{3.20}$$

i.e. a finite-dimensional matrix equation suitable for numerical solution.

Time-integration can be performed with various methods. For demonstration purposes, we show how to obtain a first-order backwards differentiation scheme by writing

$$0 = \frac{\partial f}{\partial \hat{t}} + Mf = \frac{f(t_k) - f(t_{k-1})}{\Delta t} + M(t_k) f(t_k) + \mathcal{O}(\Delta t), \tag{3.21}$$

where $t_k = k\Delta t$. Solving for $f(t_k)$ yields the implicit scheme

$$f(t_k) = \Big(I + \Delta t M(t_k)\Big)^{-1} f(t_{k-1}) + \mathcal{O}(\Delta t). \tag{3.22}$$

The only time-dependence of the operator M in our case comes from explicit variation of electric field or background plasma parameters. In a fully analogous way one can use higher order backward differentiation formulae to obtain methods with error of higher order in Δt, but stability properties differ. These will be considered in section 3.3. Common to the implicit methods is that they require the inversion of the matrix $\delta_{ij} + k\Delta t M_{ij}$ for some constant k. Due to the sparsity of M, there are efficient methods for storing and inverting the matrix, allowing matrix sizes of up to almost $10^6 \times 10^6$ on a computer with 16 GB RAM. CODION utilizes the UMFPACK [35] routine for matrix inversion.

3.2.1 Matrix elements

We will here explicitly give the matrix elements M_{ij} of our equation, where (i,j) enumerate the pairs $((n,l),(n',l'))$. This provides a complete description of the discretization of the 2D kinetic equation (3.3), in principle allowing direct implementation in any programming language.

Let us introduce the differentiation matrices corresponding to the first and second derivatives in velocity,

$$D_{n,n'} = \frac{1}{12\Delta x}\Big(- \delta_{n,n'-2} + 8\delta_{n,n'-1} - 8\delta_{n,n'+1} + \delta_{n,n'+2}\Big), \tag{3.23}$$

$$DD_{n,n'} = \frac{1}{12\Delta x^2}\Big(- \delta_{n,n'-2} + 16\delta_{n,n'-1} - 30\delta_{n,n'} + 16\delta_{n,n'+1} - \delta_{n,n'+2}\Big), \tag{3.24}$$

for all matrix elements except $n = (1, 2, n_{\max} - 1, n_{\max})$ where the standard forward and backward differentiation rules with error $\mathcal{O}(\Delta x^4)$ are used. This allows us to write M_{ij} in

the form

$$M_{ij} = \hat{E}\Bigg[\left(\frac{l+1}{2l+3}\delta_{l,l'-1} + \frac{l}{2l-1}\delta_{l,l'+1}\right)D_{n,n'} + \left(\frac{(l+1)(l+2)}{2l+3}\delta_{l,l'-1} - \frac{l(l-1)}{2l-1}\delta_{l,l'+1}\right)\frac{\delta_{n,n'}}{x_n}\Bigg]$$
$$+ \sum_b \frac{n_b Z_b^2}{n_e}\delta_{l,l'}\Bigg\{l(l+1)\delta_{n,n'}\frac{\phi(\kappa_b x_n) - G(\kappa_b x_n)}{2x_n^3} - \delta_{n,n'}\left(2\frac{T_a}{T_b}\left(2\frac{G(\kappa_b x_n)}{x_n} + \kappa_b G'(\kappa_b x_n)\right)\right.$$
$$\left. - \left(2\frac{T_a}{T_b}G(\kappa_b x_n) + \frac{G(\kappa_b x_n)}{x_n^2} + \kappa_b\frac{G'(\kappa_b x_n)}{x_n}\right)D_{n,n'} - \frac{G(\kappa_b x_n)}{x_n}DD_{n,n'}\right)\Bigg\}$$
$$- \frac{n_a Z_a^2}{n_e}\Bigg[4\delta_{l,1}\delta_{l',1}G(x_n)\frac{w_{n'}x_{n'}^2 G(x_{n'})}{\sum_m w_m x_m^3 G(x_m)\exp(-x_m^2)}$$
$$+ \delta_{l,0}\delta_{l',0}\left(8x_n G(x_n) - \frac{\phi(x_n)}{x_n}\right)\frac{w_{n'}(4x_{n'}^3 G(x_{n'}) - x_{n'}\phi(x_{n'}))}{\sum_m w_m(4x_m^5 G(x_m) - x_m^3\phi(x_m))\exp(-x_m^2)}\Bigg]\exp(-x_n^2), \tag{3.25}$$

except for the $l = l_{\max}$ elements, where the $\delta_{l,l'-1}$ terms are 0 to enforce the boundary condition.

Figure 3.1 shows the structure of the matrix, employing the enumeration $i = ((l_1,n_1),(l_1,n_2),(l_1,n_3),...,(l_2,n_1),(l_2,n_2),...)$, which is the choice made for our implementation. The two solid blocks correspond to the integrals appearing in the conserving terms in the field-particle self collision operator. Lines correspond to velocity derivatives, and each have a width of five matrix elements, while the three different lines correspond to the factor $\delta_{l,l'\pm1}$ appearing in the electric field-term: this term is responsible for driving the anisotropy of the distribution, while collisions with the bulk act to restore spherical symmetry.

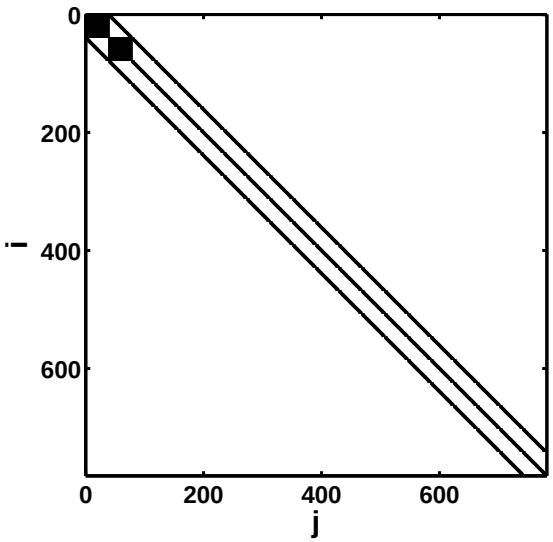

Figure 3.1: Non-zero matrix elements of M_{ij}. For this demonstration we have chosen parameters $n_{\max} = 40$ and $l_{\max} = 20$; larger values are typically needed for solutions to converge. The solid blocks correspond to the integral moments of the distribution appearing in the self-collision model operator, and the lines correspond to velocity derivatives. The existence of three lines is due to the directional electric field.

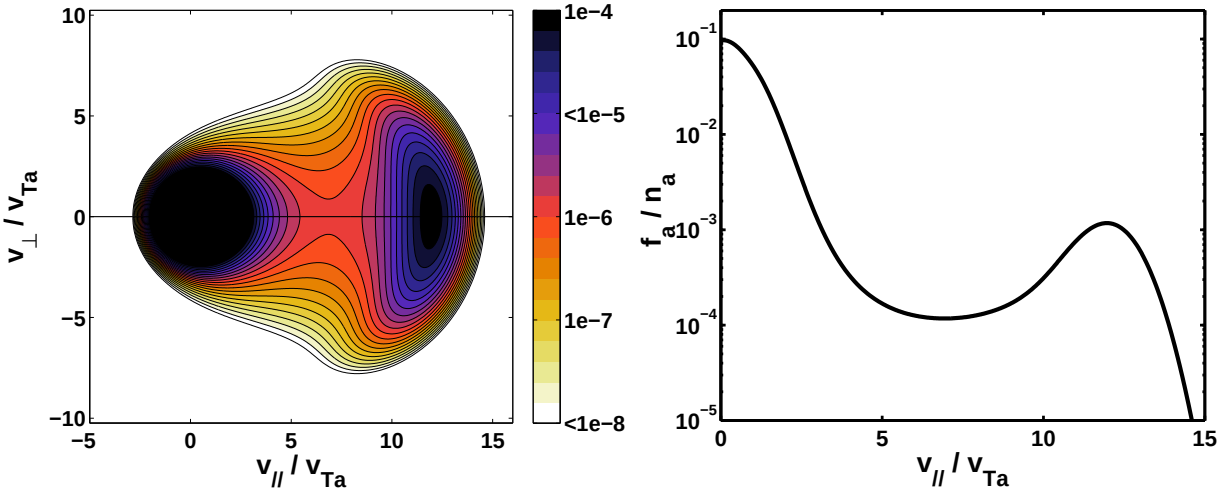

Figure 3.2: Distribution function $f_a(\mathbf{v})/n_a$ of deuterium for the test-case with effective electric field $E^*/E_D = 0.08$ at time $t = 1000\tau_{ae}$. This is the reference distribution used for the convergence tests presented in this section. We use $v_\parallel = \xi v$ and $v_\perp = \pm\sqrt{1-\xi^2}v$. The figure to the right shows the $\xi = 1$ ($v_\perp = 0$) cut of the distribution function.

3.3 Convergence

In this section we shall investigate the convergence properties of the solution with respect to the various grid parameters. As a measure of error we will use the functional

$$||\Delta f|| = \frac{\int \mathrm{d}^3\mathbf{x}\,|f(\mathbf{x}) - \bar{f}(\mathbf{x})|^2}{\int \mathrm{d}^3\mathbf{x}\,|\bar{f}(\mathbf{x})|^2}, \tag{3.26}$$

where $\bar{f}$ is a reference distribution, obtained using a grid where the solution is well converged. Differences between a solution and the reference distribution is barely visible for $||\Delta f|| \lesssim 10^{-4}$. The test-case will be a fully ionized deuterium plasma with carbon impurities such that $Z_{\mathrm{eff}} = 2.5$. We choose a typical effective electric field for runaway, $E^*/E_D = 0.08$, maximum velocity $x_{\max} = 20$ and time $t_{\max} = 1000\tau_{ae}$. All species will be held at the same temperature, and the momentum and energy conserving self-collision operator will be used. We solve for the distribution of deuterium, and the solution in the final time step is shown in figure 3.2. Throughout this work we will show $\xi = 1$ ($v_\perp = 0$) cuts of the distribution function, since this represents the direction in which the electric field accelerates the ions. Along this line the build-up of a fast ion population will be most strongly pronounced. A significant fast ion population is seen to form in this case, accumulating near $v = 12v_{Ta}$.

Convergence of the solution with respect to time-step is shown in figure 3.3. Of the three methods shown, the first order implicit Euler method (BDF1) consistently gives the best results for a large range of time-steps. For $||\Delta f|| < 10^{-4}$, it is seen that time steps smaller than ~ 50 collision times is sufficient with this scheme. However, with a sufficiently accurate velocity grid discretization, conservation properties become independent of time step as discussed in the next section, allowing one to use time steps of millions of collision times for certain applications (for example studying time-asymptotic behaviour to find steady-state distributions). As implicit Euler (BDF1) consistently provides good results with no indication of significant improvement with higher-order schemes, this scheme has been chosen for the results presented in this thesis.

Convergence with respect to $l_{\max}$ and Δx is presented in figure 3.4. The solution converges extremely rapidly with respect to $l_{\max}$, and no additional accuracy is obtained after $l_{\max} = 30$ for this case. Certain scenarios can require higher $l_{\max}$; the required value is closely related to the width of the distribution function in ξ, as discussed in the previous section. Heavier ions, such as impurities, accumulate at larger v/v_{Ti}, with the consequence that the runaway distribution becomes highly anisotropic. To resolve such a distribution, $l_{\max}$ of order 200 or more can be needed. Figure 3.4 (b) showing convergence with respect to grid step Δx illustrates the power law dependence of the error. For grid steps Δx larger than 0.1 the solutions quickly diverge, while grid steps significantly smaller than 0.1 are only needed for long simulations requiring high precision in the conservation of particle number.

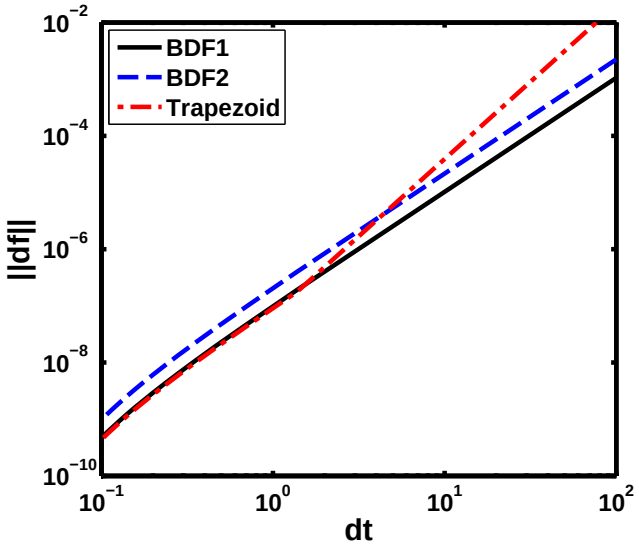

Figure 3.3: Error as function of time step size Δt for different time integration methods. BDF1 and BDF2 denote the first and second order backwards differentiation formulae respectively, and "Trapezoid" denotes the integration method based on the second order trapezoid rule.

3.4 Conservation properties

The 2D kinetic equation (Eq. (3.3)) which is solved in CODION obeys certain analytic conservation laws: density conservation, and conservation of momentum and energy in self-collisions. In this section we will consider how these are affected by discretization, and with the numerical solution evaluate how well they are satisfied with our discretization scheme.

Density, momentum and energy are integral moments of the distribution f, which we denote generally here by w. In vector form they can be written

$$w = u^\top f, \tag{3.27}$$

where $u^\top$ is a functional taking f to the scalar w. For an example, we have defined the density n_a as

$$n_a = \int \mathrm{d}^3\mathbf{v}\, f_a(\mathbf{v}) = 4\pi \int \mathrm{d}v\, v^2 f_0(v) \approx 4\pi \sum_n w_n v_n^2 f_0(v_n), \tag{3.28}$$

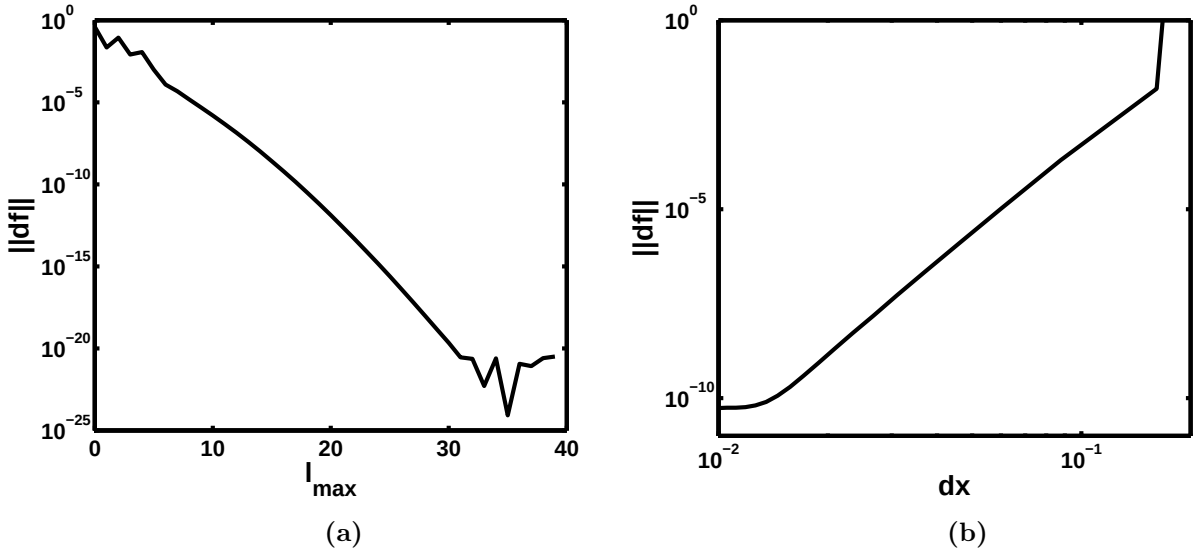

Figure 3.4: Error as function of $l_{\max}$ and Δx for the test-case. The slope of the curve in figure (a) depends on scenario, since distributions with stronger anisotropy require more Legendre modes to resolve. Figure (b) shows the error induced by the finite difference discretization scheme. Step lengths Δx at least smaller than 0.1 are needed for accurate solutions.

where w_n are the Simpson quadrature weights of Eq. (3.18), meaning that in our discretization scheme where $f_a(\mathbf{v})$ is represented by $f_l(v_n)$, the density functional corresponds to the vector

$$u_i = 4\pi w_n v_n^2 \delta_{l,0}, \tag{3.29}$$

where the index i enumerates (n,l). Consider now the kinetic equation in matrix form, Eq. (3.20): applying $u^\top$ yields

$$\frac{\partial w}{\partial \hat{t}} + u^\top M f = 0. \tag{3.30}$$

In the non-discretized problem, we have already shown in Eq. (2.40) that the differential operator M satisfies $u^\top M \equiv 0$ when $u^\top$ is the density functional, since M takes the form of a divergence, and consequently $w = n_a$ is conserved in time. In our discretization scheme, an error is induced making $u^\top M$ non-zero. However, we can estimate an upper limit of the non-conservation of density:

$$|n_a(t) - n_a(t_0)| < |t - t_0| \max(|u^\top M f|), \tag{3.31}$$

where the right-hand side denotes the maximum value $u^\top M f$ takes between t_0 and t. This implies that the conservation properties are insensitive to the time integration method and time step size. If M is an accurate discretization of the problem, the deviation of n_a from its original value will always be small, independent of time-step or scheme. Conversely, a simulation spanning larger times will generally require more accurate discretization of M to obtain the same level of conservation as a shorter simulation.

Similar considerations hold for parallel velocity X and energy W for the part of the kinetic equation (3.3) corresponding to self-collisions, where normalized velocity and energy

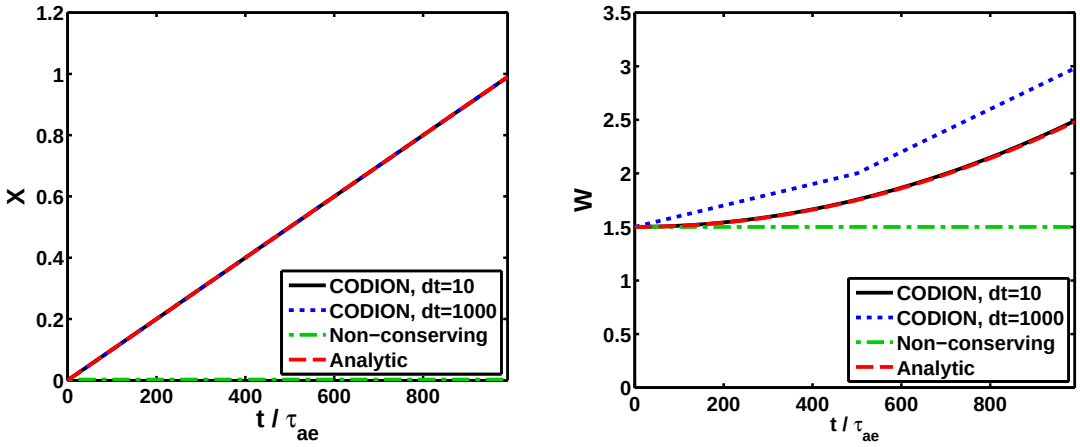

Figure 3.5: Time-evolution of the velocity and energy moments of the CODION distribution with only self-collisions accounted for, compared with the analytic result. We also show the time-evolution of the moments when the field-particle operator ensuring conservation is neglected. The left figure demonstrates excellent agreement between conserving numerical solutions and the analytic result, while all momentum is lost in the non-conserving solution. Density is conserved to 6 digits for the $\Delta t = 10$ case and to 3 digits for $\Delta t = 1000$ in the final time-step, illustrating the weak dependence of conservation on time step. For this simulation, $l_{\max} = 4$ and $\Delta x = 0.05$.

moments are defined here as

$$X = \frac{1}{n_a v_{Ta}} \int \mathrm{d}^3\mathbf{v}\, v\xi f_a(\mathbf{v}),$$
$$W = \frac{1}{n_a (m_a v_{Ta}^2/2)} \int \mathrm{d}^3\mathbf{v}\, \frac{m_a v^2}{2} f_a(\mathbf{v}). \tag{3.32}$$

Applying these integral moments to the kinetic equation with only self-collisions accounted for (neglecting electron and impurity scattering), Eq. (3.3) takes the form

$$\frac{\partial X}{\partial \hat{t}} = \hat{E}, \tag{3.33}$$
$$\frac{\partial W}{\partial \hat{t}} = 2\hat{E}X. \tag{3.34}$$

These can be integrated, yielding

$$X(\hat{t}) = X(0) + \hat{E}\hat{t} = \hat{E}\hat{t}, \tag{3.35}$$
$$W(\hat{t}) = W(0) + \hat{E}^2\hat{t}^2 = \frac{3}{2} + \hat{E}^2\hat{t}^2, \tag{3.36}$$

where we have used the initial values determined by the equilibrium distribution $f_a \propto \exp(-x^2)$. Figure 3.5 demonstrates how these analytic results compare with the corresponding moments of f_a for the CODION solution, for a test-case with normalized electric field $\hat{E} = 10^{-3}$ at time $\hat{t}_{\max} = 10^3$, such that $\hat{E}\hat{t} = 1$, with only self-collisions accounted for. For comparison, the evolution of the moments when the field-particle term is neglected is also shown. The figure further compares the case when the entire time-range is covered in one time step and when 100 time steps are used. In this scenario, the correct velocity dynamics is obtained independently of time-step, while the energy (which has a non-linear dependence on time) is sensitive to time-step. When the restoring pieces of the collision

operator ensuring conservation are neglected, the distribution is negligibly perturbed, all momentum and energy being lost in the collisions.

Note the low value $l_{\max} = 4$ used, highlighting the fact that density, velocity and energy dynamics are independent of the higher order Legendre modes. If $l_{\max}$ is too low to accurately resolve the distribution, it can affect the long time evolution of the distribution and therefore also the moments. However, higher modes $l > 2$ can never affect properties which are local in time, such as the conservation properties.

3.5 Effect of field-particle self collision operator on ion runaway distribution

In this section we investigate the effect of the model operator for field-particle self-collisions on the ion runaway distribution. The model operator consists of two terms, independent of each other: a momentum-restoring piece and an energy-restoring piece. By removing either or both of these terms, we can evaluate the effect of momentum conservation and energy conservation in self-collisions on ion runaway.

Solutions obtained for a test-case with the four different possible choices for the model operator are shown in figure 3.6, for two different plasma compositions and E-fields. Both cases are fully ionized deuterium plasmas with carbon impurities, taking the same temperature for all species and showing the deuterium distribution function evolved from a Maxwellian at $t = 0$ until the time $t = 500\tau_{ae}$. Throughout this work we will show distribution functions normalized to the density $n_a = \int \mathrm{d}^3\mathbf{v}\, f_a$.

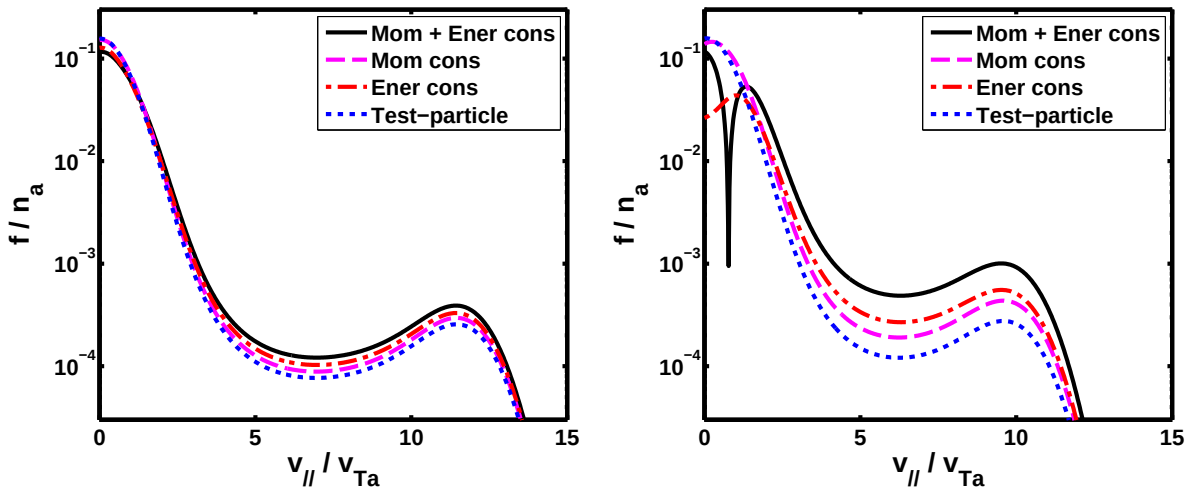

(a) $Z_{\text{eff}} = 2.5$, $E^*/E_D = 0.08$. **(b)** $Z_{\text{eff}} = 1.5$, $E^*/E_D = 0.07$.

Figure 3.6: Comparison of ion runaway distributions for choices of field-particle self-collision operator with different conservation properties (momentum and/or energy conservation). Both figures depict the $\xi = 1$ cut of the distribution of deuterium at a time $t = 500\tau_{ae}$, evolved from an initial equilibrium Maxwellian in a fully ionized deuterium plasma with carbon impurities and all species at the same temperature. For the distributions in figure (a), the solution corresponding to the test-particle operator has a runaway density $n_r = 0.06$ and the momentum and energy conserving operator $n_r = 0.09$. In figure (b), the test-particle case had $n_r = 0.04$, and the fully conserving one $n_r = 0.16$.

The parameters used are not based on any particular physical scenario, but are chosen

to illustrate the general behaviour of the solutions. The E-fields are chosen so that the case with no field-particle operator would have a runaway density $n_r \sim 0.05$, where we define a normalized runaway density

$$n_r \equiv \frac{1}{n_a} \int_{v>v_{c1}} \mathrm{d}^3\mathbf{v}\, f_a, \tag{3.37}$$

which we will use throughout this work as a measure of the fast ion population. The condition $n_r = 5\%$ at $\hat{t} = 500$ corresponds to values of the electric field $E^* = 0.07E_D$ for the $Z_{\mathrm{eff}} = 1.5$ case and $E^* = 0.08E_D$ for the $Z_{\mathrm{eff}} = 2.5$ case.

It is clear that in the scenario shown, inclusion of momentum or energy-restoring pieces increase the rate at which the runaways are generated. There is no large qualitative change in the behaviour of the fast ions – as could be expected since the field-particle operator acts mainly on the bulk. However, when Z_{eff} is near one or the density of runaways (and therefore also the perturbation $f_{a1} = f_a - f_{a0}$ of the distribution) sufficiently large, the bulk is deformed significantly. Figure 3.6 (b) shows a distribution which takes negative values for $v < v_{Ta}$. This signifies that the linearization of the collision operator is no longer valid.

To understand this behavior, we may take a closer look at the momentum and energy-restoring pieces of the self-collision field-particle operator, Eq. (2.97). It is seen that the momentum-restoring piece has the effect of removing particles from $-\mathbf{v}$ and adding them at $\mathbf{v}$, at a rate which does not depend on the value of the distribution at $\mathbf{v}$, but only a moment (weighted integral) of the distribution. This has the consequence that if the distribution is significantly perturbed (in the positive parallel direction), this term can cause negative values of the distribution at negative ξ, typically at $v \sim v_{Ta}$ where the momentum-restoring term peaks.

Similarly, the energy-restoring piece removes particles from near $v = 0$ and adds them isotropically at larger v. This again has the consequence that in the case of sufficiently large perturbations, the low-velocity bulk distribution can be significantly deformed – as is clearly demonstrated in the figure. As expected, the two energy-conserving operators exhibit this behaviour.

The presence of impurities may counter this effect, as collisional diffusion can ensure that the distortion is minimal. This limits the application of the conserving self-collision operator to cases where Z_{eff} (a measure of impurity content) is sufficiently high. Simulation shows that to obtain a distribution of runaway density $n_r \sim 0.05$ without significant distortion, values of order $Z_{\mathrm{eff}} \sim 1.8$ are typically needed. Only using the momentum-restoring piece gives a less strict requirement, with reasonable runaway distributions obtained (with a small negative bump near $v_\parallel = -v_{Ta}$) for $Z_{\mathrm{eff}} \gtrsim 1.4$. Note that these effects are a consequence of using a linearized collision operator. A non-linear treatment would allow the study of any parameter regime where the 2D kinetic equation is valid.

For some of the applications in this thesis where Z_{eff} is small, the negligence of the restoring terms will be motivated by the fact that they do not significantly affect the shape of the runaway distribution, but mainly the rate at which it builds up. It will be explicitly stated whenever this simplification is used.

3.6 Comparison of CODION with analytic solution

A time-dependent analytic solution of the ion kinetic equation was originally derived by Helander *et al.* [19] for trace impurities and generalized to arbitrary plasma composition by Fülöp and Newton [20]. A detailed derivation is presented in Appendix A. In terms of

CODION-normalized parameters, the solution is given by

$$f_{RI} \propto \exp\left[-x^2 + \frac{\hat{E}x^4}{2\bar{n}}\left(1 - \left(1 - \frac{3\bar{n}\hat{t}}{x^3}\right)^{4/3} H\left(1 - \frac{3\bar{n}\hat{t}}{x^3}\right)\right)\right], \tag{3.38}$$

where $H(x)$ is the Heaviside step function characterized by $H(x > 0) = 1$ and $H(x < 0) = 0$, obtained as the leading order term in an asymptotic expansion of the kinetic equation in $\hat{E}$. The solution is valid at $\xi = 1$, for velocities small enough that

$$x \ll \sqrt{\bar{n}/\hat{E}} = \frac{1}{\sqrt{1 + Z_{\text{eff}}/\bar{n}}} \frac{v_{c1}}{v_{Ta}}, \tag{3.39}$$

with v_{c1} given by Eq. (2.120), and times small enough that the solution can be considered a small perturbation of a Maxwellian.

It is clear that this solution describes only the initial evolution of the bulk distribution. Higher order corrections to f_{RI} in $\hat{E}$ indicate that the angular dependence of f_{RI} to leading order is given by

$$f_{RI}(v, \xi) \propto F(v) \exp\left(\sqrt{\frac{\hat{E}}{Z_{\text{eff}}}} x^2 \sqrt{1 + \xi}\right), \tag{3.40}$$

showing that it is peaked in the forward direction. However, other spherically symmetric contributions appearing at this order are unknown, meaning that we cannot consistently include the angular term when evaluating the analytic expression.

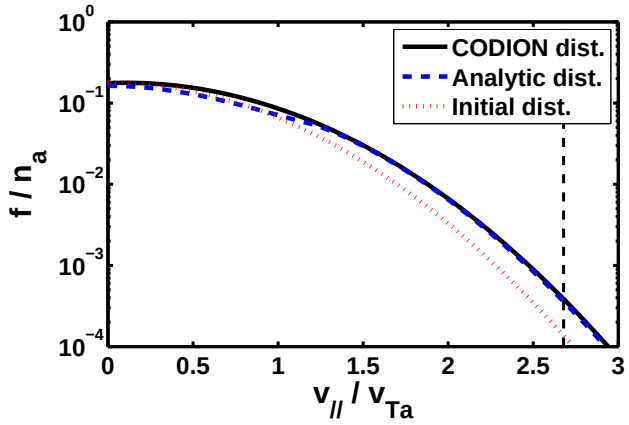

Figure 3.7: Comparison of a distribution function obtained with CODION with the analytic solution after $t = 1\,\text{ms}$ in a fully ionized deuterium plasma with main impurity carbon, characterized by $T = 1\,\text{keV}$, $n_e = 2 \cdot 10^{19}\,\text{m}^{-3}$ and $Z_{\text{eff}} = 1.2$. The vertical dashed line marks the analytic threshold runaway velocity v_{c1}, at which the analytic solution is formally no longer valid.

For the comparison we choose parameters that correspond to typical operational plasma parameters for a hot tokamak plasma. For this we use a fully ionized deuterium plasma with carbon of density $n_C = 0.04 n_D$ as the main impurity, such that the effective charge is $Z_{\text{eff}} = 1.2$. We further choose electron density $n_e = 2 \cdot 10^{19}\,\text{m}^{-3}$ and temperature $T = 1\,\text{keV}$ for all particle species. To produce a clear comparison we choose a larger than realistic constant electric field of $E = 8.7\ \text{V/m}$ corresponding to $E^*/E_D = 0.17$. Figure 3.7 shows both the normalized analytic solution and the CODION solution after $t = 1\,\text{ms}$. The agreement for the tail of the distribution is excellent. Note however that the analytic solution is never valid in the runaway region $v > v_{c1}$, limiting its use in the physical scenarios that we will consider.

Electron runaway distribution

By setting $E^* = E$, we may solve the electron kinetic equation in the non-relativistic limit. CODION can therefore also be used to obtain the runaway electron distribution function for cold plasmas, allowing a direct comparison with CODE. A comparison for a $T = 10\,\mathrm{eV}$, fully ionized pure deuterium plasma is shown in figure 3.8, with electric field $E = 0.05E_D$ at time $t = 500\tau_{ee}$. In a cold plasma such as this, the relativistic collision operator employed in CODE reduces to one similar to ours, and good agreement is expected. For the comparison, field-particle self-collisions have been neglected.

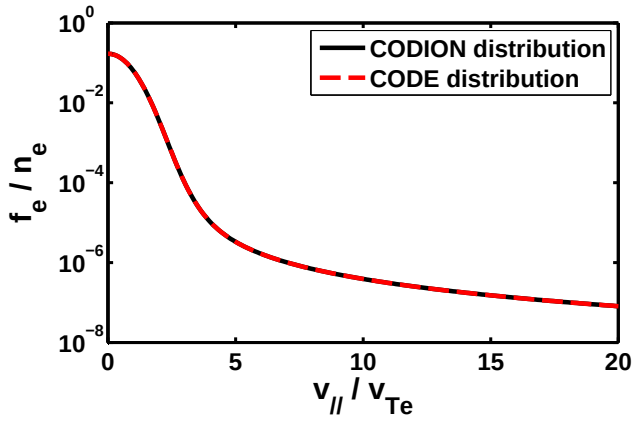

Figure 3.8: Comparison of the zeroth Legendre mode f_0 of the CODION-obtained electron distribution with the one from CODE, after a time $t = 500\tau_{ee}$ with $E/E_D = 0.05$ and $Z_{\mathrm{eff}} = 1$.

3.7 Runaway ion velocity

We will now consider the velocity that runaway ions achieve. We can define a 'peak ion velocity' v_m as that velocity at which the fast ion distribution takes its maximum value in steady-state (i.e. the largest velocity at which $\partial f/\partial v$ vanishes). Considering force-balance on a test-particle, this would be expected to be near the velocity v_{c2} estimated in Eq. (2.121). Figure 3.9 shows how v_m, v_{c1} and v_{c2} depend on E/E_c, where the critical velocities have been calculated numerically from the full test-particle force balance equation $F_c(v) - F_E(v) = 0$, with F_c and F_E given by Eqs. (2.111) and (2.109), respectively. For comparison, the figure also shows the analytical values of v_{c1} and v_{c2}, derived under the assumption that the velocities are well separated. This is reflected in the figure, since they deviate significantly from the exact values near $E = E_c$.

When $E < E_c$, the numerical values of v_{c1} and v_{c2} are both taken to be that velocity which minimizes the test-particle friction force $F_c(v)$. The runaway ion peak velocity v_m is calculated for the deuterium population in a fully ionized deuterium plasma with carbon impurities such that $Z_{\mathrm{eff}} = 2.5$, using only the test-particle collision operator (neglecting the momentum and energy restoring field-particle self collision terms). To represent the steady-state, we have evaluated the distribution functions at $t = 10^5\tau_{ae}$. It is clear from the figure that the test-particle picture breaks down for electric fields near the critical field, with ions being accelerated by electric fields significantly smaller than the critical field. The deviation can be ascribed to the diffusive nature of collisions, which is not accounted for in the test-particle picture. A positive velocity gradient forms in the steady-state fast

ion distribution already for $E > 0.81E_c$, but for $E > E_c$ the fast ion distribution peaks near v_{c2}.

It should be noted that for the larger of the electric fields shown, a very large fraction of the ion distribution sits in the runaway region in steady-state. While the physical model is not valid in such a scenario, the solutions still illustrate the accumulation point of the fast ions, which is not sensitive to the fraction of ions in the runaway region.

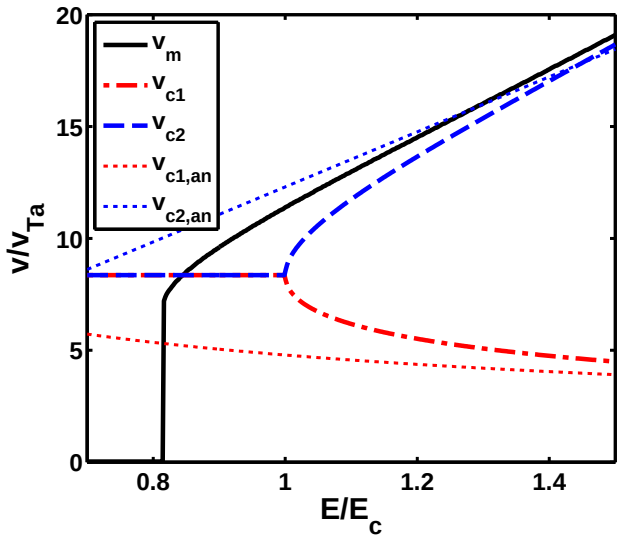

Figure 3.9: Peak runaway ion velocity v_m as function of E/E_c in steady-state for a fully ionized deuterium plasma with $Z_{\text{eff}} = 2.5$ due to carbon impurities, together with test-particle critical velocities v_{c1} and v_{c2}. Shown for comparison are also the analytic expressions $v_{c1,an}$ and $v_{c2,an}$ of the critical velocities.

Chapter 4

Applications

In this chapter CODION is applied to calculate runaway ion distributions for typical fusion and space plasmas. The rate at which a fast ion population forms due to the runaway mechanism is determined, and it is investigated whether the difference in acceleration rate between different ion species can explain the enhanced abundance of heavy ions in the solar wind. We will consider the possibility of Alfvénic instabilities being driven by runaway ions during tokamak disruptions. For the tokamak plasmas we will investigate scenarios with parameters characteristic of the TEXTOR [36], JET [37] and (future) ITER [38] tokamaks.

4.1 Runaway ion distributions

In this section we will demonstrate typical runaway ion distributions for three different physical scenarios: hot fusion plamas, cold disruption-like tokamak plasmas and solar flare plasmas. The scenarios shown are such that the runaway density defined in Eq. (3.37) is $n_r = 0.05$, which is small enough that the solutions are within the domain of validity of our linearized model.

4.1.1 Hot tokamak plasma

The hot tokamak cases represent plasmas with typical operational parameters of today's experiments. We will first consider plasma parameters typical for the TEXTOR tokamak during flat-top operation: The plasma composition is deuterium, with fully ionized carbon as main impurity. The density of carbon is set to obtain the desired value of the effective charge $Z_{\text{eff}} = \sum_i n_i Z_i^2/n_e = 2$ [39], corresponding to $n_C = 0.042 n_D$. The electron density is $n_e = 3 \cdot 10^{19}\,\text{m}^{-3}$, and all particle species in the plasma are assumed to have the same temperature $T = 1\,\text{keV}$ [40, 41].

During steady-state flat-top operation, the average electric field in the plasma can be estimated using the Spitzer resistivity,

$$E = \eta j \sim \eta \frac{I}{\pi a^2} \tag{4.1}$$

where I is the total toroidal current, a the minor radius of the plasma and

$$\eta = \sqrt{\frac{\pi}{2}} \frac{Z_{\text{eff}}}{4} \ln\Lambda \frac{e^2\sqrt{m_e}}{(4\pi\varepsilon_0)^2 T_e^{3/2}} \tag{4.2}$$

is the Spitzer resistivity [16]. Assuming a plasma current of $I = 350\,\text{kA}$ [40] and minor radius $a = 0.4\,\text{m}$ characteristic of TEXTOR, we obtain a typical average electric field

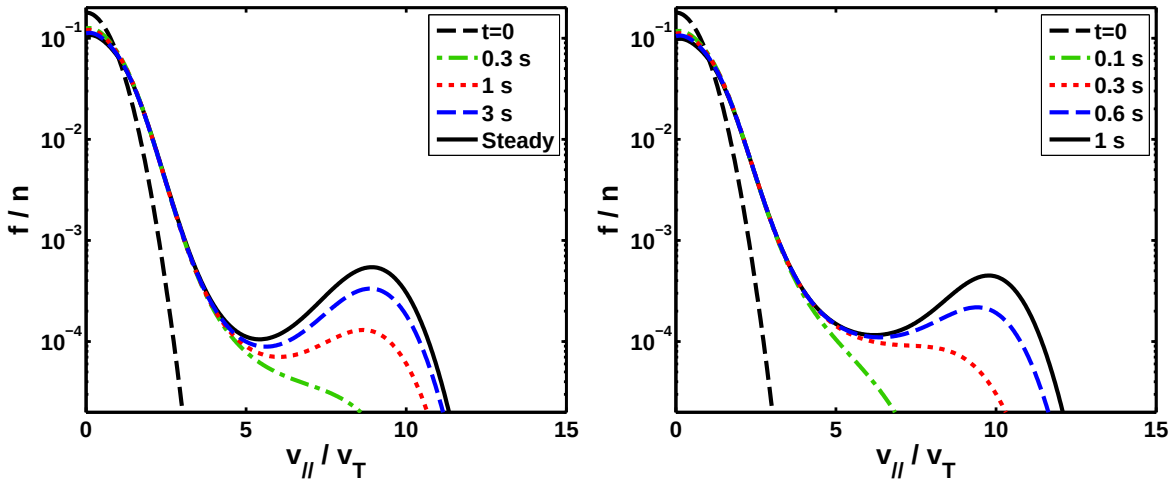

(a) $E = 1.64\,\mathrm{V/m}$. **(b)** $E = 1.75\,\mathrm{V/m}$.

Figure 4.1: Time-evolution of the deuterium distribution for typical TEXTOR operating parameters: temperature $T = 1\,\mathrm{keV}$ for all particle species; electron density $n_e = 3 \cdot 10^{19}\,\mathrm{m}^{-3}$; Effective charge $Z_{\mathrm{eff}} = 2$ caused by fully ionized carbon as main impurity. The electric fields are enhanced, compared to standard operating values. Both cases shown are characterized by a runaway density $n_r = 0.05$ in the final state. $E = 1.64\,\mathrm{V/m}$ corresponds to $E/E_D = 0.13$ and $E/E_c = 0.89$, while $E = 1.75\,\mathrm{V/m}$ corresponds to $E/E_D = 0.14$ and $E/E_c = 0.95$.

of $E = 0.007\,\mathrm{V/m}$. This corresponds to $E/E_D = 5 \cdot 10^{-4}$ and $E/E_c = 0.004$. This is of order 250 times too low for ions to be significantly accelerated; even accounting for radial profiles, it is unlikely that electric fields near the required value for ion runaway ($E \sim 0.8E_c = 1.5\,\mathrm{V/m}$) will occur anywhere in the plasma during standard operation.

Performing a similar analysis for the ITER tokamak with plasma parameters consistent with [42, 43], taking electron density $n_e = 10^{20}\,\mathrm{m}^{-3}$, temperature $T = 20\,\mathrm{keV}$ for all species, major radius $a = 2\,\mathrm{m}$, plasma current $I = 15\,\mathrm{MA}$ and effective charge $Z_{\mathrm{eff}} = 2$, we obtain from the resistivity estimate an average electric field $E = 1.6 \cdot 10^{-4}\,\mathrm{V/m}$ corresponding to $E/E_D = 6 \cdot 10^{-5}$ and $E/E_c = 4 \cdot 10^{-4}$. The high temperature of the ITER plasma causes the required electric field to sustain the plasma current to be low, while the high electron density causes the ion critical field E_c to be relatively high. Because of this we obtain values of E/E_c thousands of times smaller than that required for runaway to occur during standard operation in an ITER-like burning plasma.

Finally performing the same analysis for the JET tokamak, using characteristic plasma parameters $n_e = 3 \cdot 10^{19}\,\mathrm{m}^{-3}$, temperature $T = 3\,\mathrm{keV}$ for all species, plasma current $I = 2\,\mathrm{MA}$, effective charge $Z_{\mathrm{eff}} = 2$ and minor radius $a = 1\,\mathrm{m}$ consistent with [42], we obtain from Eq. (4.1) an average electric field $E = 0.0013\,\mathrm{V/m}$, $E/E_D = 3 \cdot 10^{-4}$ and $E/E_c = 0.002$, also here significantly lower than that required to accelerate ions.

However, large electric fields can sometimes be induced by sudden cooling in connection with instabilities in the plasma. There is experimental evidence for acceleration of electrons in connection with sawtooth instabilities in JET [44, 45] indicating the possibility of elevated electric fields causing runaway. Reconnection events in MAST are also known to cause significantly increased electric fields of order tens of V/m, lasting for a few milliseconds [19]. It is therefore of interest to investigate the time-scales for the acceleration of ions in hot fusion plasmas with enhanced electric fields.

In figure 4.1 we show the time-evolution of the $\xi = 1$ cut of the fast ion distribution in a plasma with parameters typical of the TEXTOR tokamak, with electric field near the

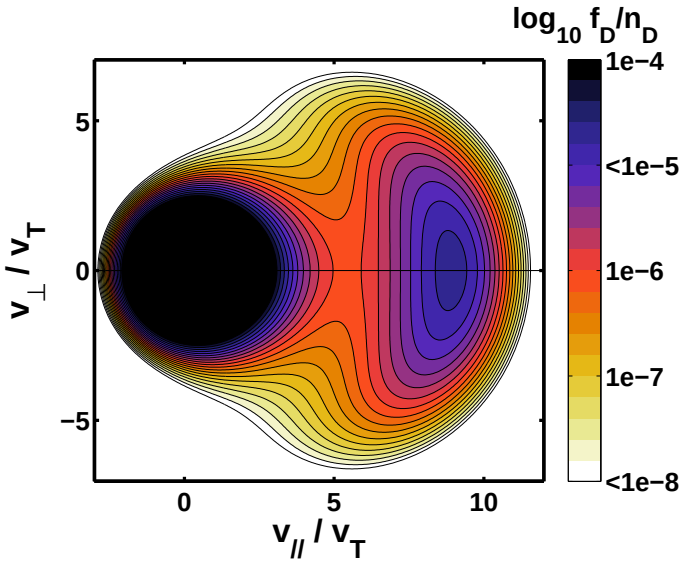

Figure 4.2: Contour plot of the steady-state deuterium distribution function f_D in a TEXTOR-like plasma, with $n_e = 3 \cdot 10^{19}\,\mathrm{m}^{-3}$, $T = 1\,\mathrm{keV}$, $Z_{\mathrm{eff}} = 2$ and $E = 1.64\,\mathrm{V/m}$.

ion critical field E_c, for two cases. In the first case, the electric field was chosen to yield a runaway density $n_r = 5\%$ in the steady-state solution, corresponding to $E = 1.64\,\mathrm{V/m}$. In the second case, it was chosen so that $n_r = 5\%$ after 1 s, corresponding to an electric field $E = 1.75\,\mathrm{V/m}$. The time-scale of acceleration is seen to be of order seconds, which means that electric fields caused by instabilities lasting for millisecond time scales will not accelerate ions by the runaway mechanism considered in this work. In a larger tokamak such as ITER for the corresponding situation with electric field $E \sim E_c$ near the ion critical field, the time-scale of acceleration is of order four times faster than the TEXTOR case. This is still significantly longer than the time-scale of instabilities (milliseconds), meaning that the same conclusion holds for large tokamaks. A 2D plot in the velocity plane of the deuterium distribution function is shown in figure 4.2 for the steady-state solution of the TEXTOR case.

It is important to point out that we model all scenarios as a static acceleration from an initial Maxwellian. Since plasma conditions can rapidly change on a time scale of a few collision times during instabilities or disruptions, it is not certain that the initial distribution is accurately described by a Maxwellian. So-called "hot-tail" generation has been shown to be an important effect for electron runaway, where a seed of runaway electrons are provided by fast electrons present before cooling [51]. These fast electrons are cooled at a slower rate than the low-energy electrons, and may find themselves in the runaway region when the plasma has reached its final temperature. Hot-tail ions have not been considered in this work, although our model allows such a study. Finally the electric field also varies in time, which we have represented with a constant representative value in lack of accurate measurement data.

Note finally that the 2D ion kinetic equation (2.108) is not strictly valid in this scenario, where we have neglected all effects related to spatial variation of the plasma. We have previously argued that these terms contribute to the kinetic equation at a characteristic frequency v/L, with v the ion velocity and L a typical length-scale of variation of the plasma along the parallel direction. The terms were neglected when compared to the collision frequency ν_{ae} and the acceleration time-scales. With an optimistic parallel length-

scale $L \sim 2\pi R_0 \sim 10\,\mathrm{m}$ for the TEXTOR case and $L \sim 40\,\mathrm{m}$ for the ITER case, and taking the thermal velocity $v \sim v_{Ta} = \sqrt{2T_a/m_a}$, we obtain a frequency of order $v/L \sim 10^4\,\mathrm{s}^{-1}$ in both the TEXTOR and the ITER cases. This can be compared to the collision frequency ν_{ae} which is of order $10^3\,\mathrm{s}^{-1}$ for TEXTOR and of order $50\,\mathrm{s}^{-1}$ for ITER at the temperatures and densities used here. Rather than being negligible, spatial effects are expected to be significant in this scenario. Note that thermal velocity scales with temperature as $v_T \propto T^{1/2}$ while collision frequency as $\nu_{ae} \propto n_e/T^{3/2}$, indicating that the model becomes increasingly accurate at lower temperatures or higher densities, where collisions dominate.

4.1.2 Cold tokamak plasma

The cold tokamak case represents a post-disruption plasma. Disruptions are events where the plasma is rapidly cooled, typically reducing the temperature from operating temperature to a few eV within a time frame of milliseconds. This is associated with a dramatic increase in plasma resistivity, causing large electric fields to be induced [6, 46], typically lasting for a few ms. In such a scenario, large electron runaway currents can form, with potential to cause serious damage to plasma-facing components of the tokamak.

To investigate a potential electron runaway mitigation system, experiments have been performed where massive amounts of argon gas was injected into the confinement chamber, showing reduced electron runaway generation in some cases [41, 47]. In this section we will consider the evolution of the ion distribution function under conditions typical for such experiments performed at TEXTOR [41]. To model this, we will assume a plasma composition such as that used for the previous hot scenario – $n_C = 0.042 n_D$. However, in the post-disruption plasma, there will be an additional density of argon, and temperatures will be lower with the consequence that impurity ions are not fully ionized. Argon gas of order 100 times the density of the initial electron density was injected during the experiments, but only a small fraction is expected to reach the core of the plasma [41, 47]. We will take $n_{Ar} = 0.2 n_D$ as a typical argon density for the post-disruption scenario.

Typical electric fields in a TEXTOR post-disruption plasma are estimated to be of the order a few tens of V/m, lasting for a few milliseconds [48]. Figure 4.3 illustrates the dependence of the ion critical electric field E_c, calculated numerically from Eq. (2.111), on plasma temperature (all species assumed to be at the same temperature) and deuterium density assuming that all carbon and argon impurities have charge number $Z = 2$ for all temperatures. The ionization energy of the second electron is 24 eV for carbon and 28 eV for argon [50], indicating that at temperatures significantly lower than 20 eV the effective charge Z_{eff} will be close to unity, causing E_c to increase significantly (not represented in figure 4.3) under such conditions.

Although often poorly diagnosed, temperatures in the post-disruption plasma are expected to be in the sub-10 eV range, with the consequence that the critical field E_c will be greater than 50 V/m for $n_D \gtrsim 5 \cdot 10^{18}\,\mathrm{m}^{-3}$, even in the case with $Z = 2$ impurities, as can be seen in figure 4.3. While post-disruption measurements are unavailable for the TEXTOR experiments, measurements show a drop in core plasma density in connection with the disruption [41]. Assuming a deuterium density $n_D = 1 \cdot 10^{19}\,\mathrm{m}^{-3}$, realistic post-disruption electric fields (of order 30 V/m) will only accelerate ions with temperature $T \gtrsim 20\,\mathrm{eV}$.

In larger tokamaks such as ITER, models indicate that larger electric fields of order 100 V/m may be induced for several milliseconds during disruptions [49]. However, with deuterium densities of order $n_D \sim 10^{20}\,\mathrm{m}^{-3}$, figure 4.3 indicates that the critical electric field will be significantly larger than 100 V/m at a typical post-disruption temperature $T = 10\,\mathrm{eV}$ expected for ITER [10], even when optimistically assuming charge number

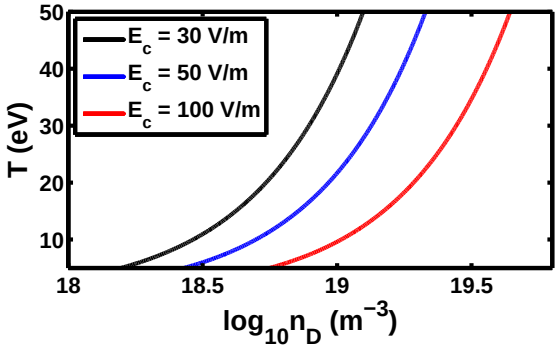

Figure 4.3: Dependence of the ion critical electric field E_c on deuterium density and plasma temperature (assumed to be the same for all particle species). The carbon density is $n_C = 0.042 n_D$ corresponding to a pre-disruption effective charge $Z_{\text{eff}} = 2$, and we have here assumed an argon density $n_{Ar} = 0.2 n_D$ to simulate a post-disruption scenario induced by massive gas injection. Charge numbers are taken as $Z_C = Z_{Ar} = 2$.

$Z = 2$ for the impurities. These considerations imply that it is unlikely that fast ions will be produced by the runaway mechanism during tokamak disruptions, unless the hot-tail mechanism is significant.

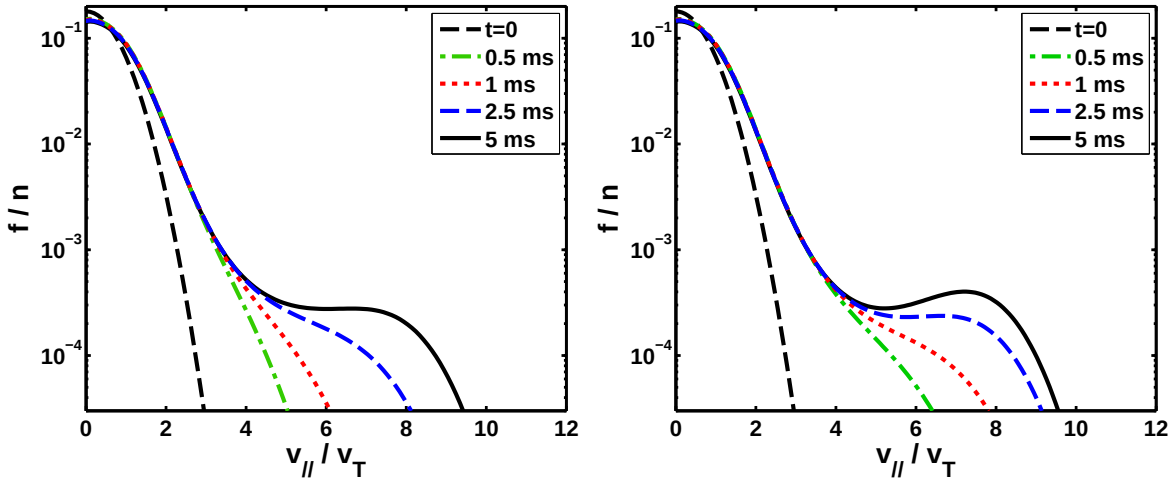

(a) TEXTOR case, $E = 40\,\text{V/m}$. **(b)** ITER case, $E = 110\,\text{V/m}$.

Figure 4.4: Time-evolution of the deuterium distribution for TEXTOR and ITER post-disruption scenarios with temperature $T = 25\,\text{eV}$. Both cases show a runaway density of $1-2\%$ after $t = 5\,\text{ms}$. Both cases use carbon density $n_C = 0.042 n_D$ and argon density $n_{Ar} = 0.2 n_D$ with $Z_C = Z_{Ar} = 2$ with a corresponding effective charge $Z_{\text{eff}} = 1.33$. For the TEXTOR case the deuterium density is $n_D = 1 \cdot 10^{19}\text{m}^{-3}$ and for the ITER case $n_D = 3 \cdot 10^{19}\text{m}^{-3}$.

We will consider ion acceleration in a TEXTOR-like and ITER-like post-disruption plasma with a higher temperature $T = 25\,\text{eV}$. This can be seen either as representing an atypical disruption case where the final plasma is hotter, or as representing the initial phase where the temperature have not yet reached its final value. A typical time scale for the cooling phase of the disruption (the "thermal quench") is one millisecond [6]. We take charge numbers $Z_C = Z_{Ar} = 2$ consistent with the ionization energies of the corresponding atoms. For the TEXTOR case we take deuterium density $n_D = 1 \cdot 10^{19}\text{m}^{-3}$, carbon density

$n_C = 0.042 n_D$ and argon density $n_{Ar} = 0.2 n_D$, corresponding to $Z_{\text{eff}} = 1.33$. ITER will use tungsten walls rather than carbon walls, and will thus not have significant amounts of carbon impurities. We will however use carbon to represent all heavier impurities for this scenario, since the results are not sensitive to which ion species is used. We therefore take the same plasma composition for the ITER case, but with $n_D = 3 \cdot 10^{19}$. This represents a core density lower by a factor 3 when compared to typical pre-disruption values. Figure 4.4 shows the time-evolution of the deuterium distribution function during 5 ms of acceleration from an initial Maxwellian with $E = 40\,\text{V/m}$ for the TEXTOR case and $E = 110\,\text{V/m}$ for the ITER case, corresponding to $E/E_c = 0.91$ and $E/E_c = 0.88$ respectively. The figure illustrates how a small fast ion population of density $n_r \sim 1 - 2\%$ forms within a few milliseconds, with a positive velocity gradient forming after $t = 5\,\text{ms}$ for the TEXTOR case and after $t = 2.5\,\text{ms}$ for the ITER case. It should be noted again that these represent extreme scenarios with temperature, electric fields and time-scales pushing the limit for what is realistic.

We can also investigate how the ion distribution at a given time varies with strength of the driving electric field. Figure 4.5 shows how the deuterium distribution evaluated after a time 3 ms of acceleration from an initial Maxwellian – a typical time scale for the induced electric field – varies with electric field for the TEXTOR case with $n_D = 1 \cdot 10^{19}\text{m}^{-3}$, $T = 25\,\text{eV}$ and plasma composition as before with $Z_{\text{eff}} = 1.33$. It is seen that in this case, for electric fields below $35\,\text{V/m}$ the initial ion distribution is only slightly perturbed. The behaviour is sensitive to which temperature is chosen for the plasma: decreased temperature increases the electric fields needed to accelerate ions, but makes the acceleration time scale shorter.

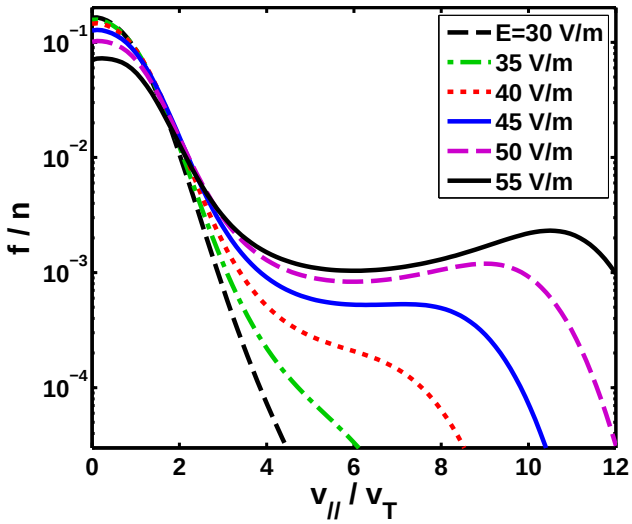

Figure 4.5: The deuterium distribution function for various electric fields after a time $t = 3\,\text{ms}$ of acceleration from an initial Maxwellian in a TEXTOR post-disruption like plasma. The deuterium density is $n_D = 1 \cdot 10^{19}\,\text{m}^{-3}$; temperature $T = 25\,\text{eV}$; carbon density $n_C = 0.042 n_D$; argon density $n_{Ar} = 0.2 n_D$. The ion critical field is $E_c = 44\,\text{V/m}$.

We can verify the validity of our model in this scenario by noting that the characteristic frequency of spatial transport at the temperature $T = 25\,\text{eV}$ is $v_T/L \sim 4.5 \cdot 10^3\,\text{s}^{-1}$, while the collision frequency is $\nu_{ae} \sim 8 \cdot 10^4\,\text{s}^{-1}$ – larger by a factor 20. This indicates that effects due to toroidicity of the system can be considered small compared to the effects of collisional dynamics considered in our model.

4.1.3 Solar flare plasma

Ion runaway has been of interest in astrophysics as a possible explanation of the experimentally measured abundances of energetic heavy ions in the solar wind [14, 52]. Ion species with larger charge number will experience a greater effective electric field $E* = (1 - Z/Z_{\text{eff}})E$, which might explain a preferential acceleration of such ions in the solar flare. With CODION we can numerically determine the time evolution of the ion distribution function and evaluate the dependence of acceleration rate on various atomic parameters.

Plasma parameters in solar flares are not well-diagnosed, but we will choose parameters consistent with the choices made by Holman [14]. We have taken a plasma temperature $T = 700\,\text{eV}$ (corresponding to 8 million Kelvin) for all particle species, and a hydrogen density $n_H = 3 \cdot 10^{17}\,\text{m}^{-3}$. The plasma composition is based on the ion abundances recommended by Schmeltz *et al.* [53]. We use a helium population of density $n_{\text{He}}/n_{\text{H}} = 6\%$, and represent all heavier impurities by a carbon population of density $n_{\text{C}}/n_{\text{H}} = 0.1\%$. This corresponds to an effective charge $Z_{\text{eff}} = 1.13$. Electric field strengths in solar flares are not constrained by experimental observation, and we will investigate the rate of acceleration at a range of values. The Dreicer field is $E_D = 224\,\text{mV/m}$ for this set of plasma parameters.

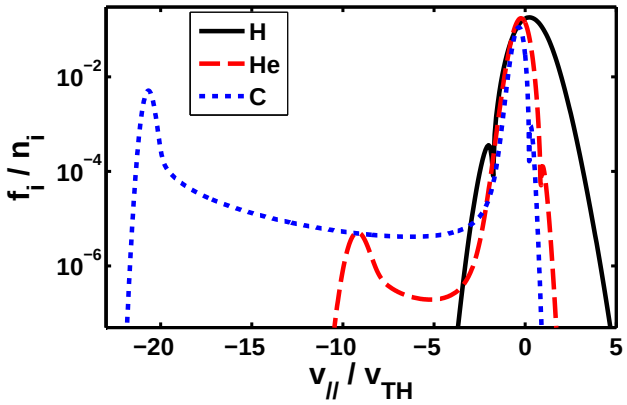

Figure 4.6: Distribution functions of hydrogen, helium and carbon after 30 s of acceleration in a solar flare-type plasma, with $E = 50\,\text{mV/m}$. All distribution functions are normalized to their respective densities. The model for self-collisions uses only the momentum-restoring term, causing small negative values of the distribution functions in the direction opposite that of acceleration. The runaway densities are $n_{r,\text{H}} \approx 0$ for hydrogen, $n_{r,\text{He}} = 3.5 \cdot 10^{-4}$ for helium and $n_{r,\text{C}} = 0.18$ for carbon.

The ion critical electric fields E_c for the plasma composition given above is $E_{c,\text{H}} = 154\,\text{mV/m}$ for hydrogen, $E_{c,\text{He}} = 40\,\text{mV/m}$ for helium and $E_{c,\text{C}} = 20\,\text{mV/m}$ for carbon. Figure 2.1 illustrates approximately how critical electric field depends on ion charge. Note that acceleration rate depends not only on E/E_c, but also on v_{c1}/v_{Ti}. Figure 4.6 shows the $v_\perp = 0$ cut of the distribution functions of hydrogen, helium and carbon after 30 s of acceleration from initial Maxwellians with the plasma parameters specified above, and an electric field $E = 50\,\text{mV/m}$. This is significantly below the hydrogen critical field, and no runaway ion population forms for the hydrogen distribution. However, fast ion populations of both helium and carbon form, with runaway densities $n_{r,\text{He}} = 0.035\%$ for helium and $n_{r,\text{C}} = 18\%$ for carbon, calculated with n_r given in Eq. (3.37). In these simulations we neglect the energy restoring self-collision term due to the low effective charge of the plasma,

and a small distortion of the bulk can be noted.

Positive values of $v_{\parallel}$ represent the direction of the electric field. Figure 4.6 therefore also illustrates how heavier ions (charge $Z > Z_{\text{eff}}$) are accelerated in the direction opposite to the electric field, pulled by electron friction. The corresponding 2D carbon distribution function is shown in figure 4.7, showing a strong anisotropy of the distribution function. The reason is that the accumulation velocity v_{c2} is located at a higher value of v/v_{Ti} for heavier ions, making pitch angle scattering of the energetic heavy ions less significant than for light ion species.

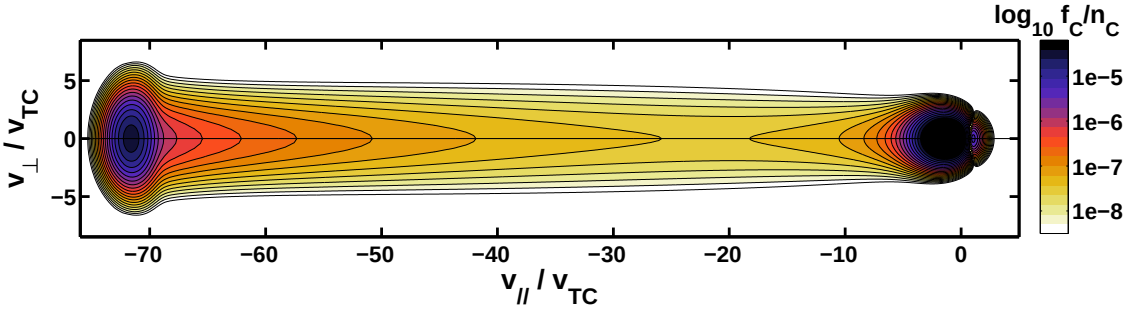

Figure 4.7: Distribution function f_C of carbon, accelerated from an initial Maxwellian for 30 s by a $E = 50\,\text{V/m}$ electric field in a solar flare-type plasma with hydrogen density $n_{\text{H}} = 3 \cdot 10^{17}\text{m}^{-3}$, helium density $n_{\text{He}}/n_{\text{H}} = 6\%$ and carbon density $n_{\text{C}}/n_{\text{H}} = 0.1\%$ (fully ionized), and temperature $T = 700\,\text{eV}$ for all species.

We will now investigate how the rate of acceleration varies with electric field strength and ion species. Figure 4.8 shows how the runaway density n_r, defined in Eq. (3.37), depends on electric field after 30 s of acceleration, for both helium and carbon. Holman [14] used an estimate for a runaway rate γ based on an analytic result due to Gurevich [12], scaling like $\gamma \propto \exp(-E_0/E)$ for some constant E_0. Figure 4.8 also shows fits of the runaway densities $n_r = n_0 \exp(-E_0/E)$ (with n_0 and E_0 both free) for $E > E_c$, where $E_c = 20\,\text{mV/m}$ and 40 mV/m for carbon and helium, respectively. It is seen that there is a fair agreement between the analytic scaling and our numerical results. However, it is difficult to define an unambiguous runaway rate for lighter ion species such as hydrogen or deuterium, where the accumulation velocity v_{c2} is closer to the thermal velocity. This has the consequence that there is no phase of the runaway process where the runaway density grows at constant rate.

We can finally determine the dependence of acceleration rate on ion charge and mass. Figure 4.9 shows the runaway density n_r after 30 s of acceleration in an $E = 40\,\text{mV/m}$ electric field, as function of ion charge Z. We have assumed a background plasma the same as above with temperature $T = 700\,\text{eV}$ and hydrogen density $n_{\text{H}} = 3 \cdot 10^{17}\,\text{m}^{-3}$, with a plasma composition of 6% helium and 0.1% carbon. To determine the runaway density of heavier ions, we have introduced trace amounts of each ion species with charge between 2 (helium) and 18 (argon), assumed to be fully ionized. Ions of charge $Z > 8$ will in reality typically not be fully ionized due to the high ionization energy, meaning that the results shown here will overestimate the acceleration rate of the heavier ions. The ion masses have been set to that of the most common isotope, i.e. we use ^{7}Li, ^{9}Be, ^{20}Ne etc. Both ^{3}He and ^{4}He are shown, with ^{3}He showing an acceleration rate a factor 60 times larger than that of ^{4}He. Ions of charge between $Z = 4$ (^{9}Be) and $Z = 8$ (^{16}O) are seen to be preferentially accelerated over lighter or heavier elements. The runaway rate decreases exponentially with ion charge for $Z > 8$. However, further studies are required to determine the effects of variation in background composition, temperature, density and

electric field on the relative rates of acceleration between ion species. The results presented here demonstrate the utility of the code for the problem.

Finally we wish to note that, while it would be of interest to investigate cases with higher electric fields, already the electric field $E = 40\,\mathrm{mV/m}$ used here corresponds to $E/E_D = 0.18$, which is large for electrons. Our model will quickly break down for higher electric fields, as the electrons – which are assumed to be in force balance between electric field and ion friction – will be rapidly accelerated by the electric field. In addition, acceleration by quasi-static electric fields is not the only mechanism for ion acceleration present in the flare plasma. Interaction with Alfvén waves can accelerate ions which have velocities above the Alfvén velocity, which is usually well above the thermal ion velocity and requires an initial acceleration by electric fields before becoming significant [13, 14]. CODION provides the means for more accurate modeling of the effects of such interactions. CODION provides a foundation on which more accurate modeling of such interactions could be based.

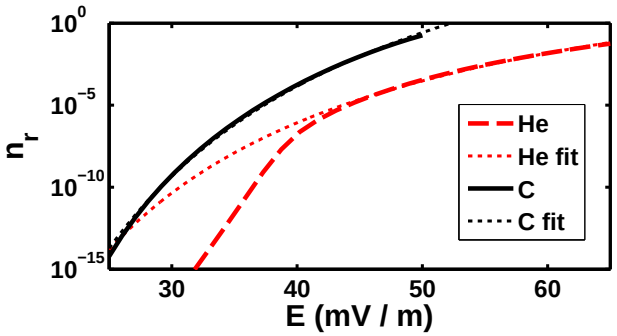

Figure 4.8: Runaway density n_r after 30 s of acceleration from an initial Maxwellian for carbon and helium, as function of electric field strength E. Shown is also fits of $n_r = n_0 \exp(-E_0/E)$ to the runaway density for $E > E_c$. The plasma composition represents a solar flare plasma and consists mainly of hydrogen with density $n_\mathrm{H} = 3 \cdot 10^{17}\,\mathrm{m}^{-3}$, with helium of density $n_\mathrm{He}/n_\mathrm{H} = 6\%$ and carbon of density $n_\mathrm{C}/n_\mathrm{H} = 0.1\%$. The temperature is $T = 700\,\mathrm{eV}$ for all particle species. Energy conservation in self-collision is not included due to the low effective charge $Z_\mathrm{eff} = 1.13$.

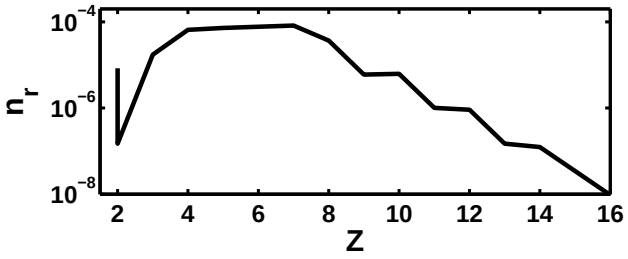

Figure 4.9: Runaway density n_r after 30 s of acceleration from an initial Maxwellian with an electric field $E = 40\,\mathrm{mV/m}$, for ion species with charge Z between 2 and 16. For each charge number the most common isotope is used, except for helium ($Z = 2$) where both ^{3}He and ^{4}He are shown, with ^{3}He having the higher runaway density. The plasma composition represents a solar flare plasma and consists mainly of hydrogen with density $n_\mathrm{H} = 3 \cdot 10^{17}\,\mathrm{m}^{-3}$, with helium of density $n_\mathrm{He}/n_\mathrm{H} = 6\%$, carbon of density $n_\mathrm{C}/n_\mathrm{H} = 0.1\%$ and trace amounts of all other species. The temperature is taken to be $T = 700\,\mathrm{eV}$ for all particle species.

4.2 TAE growth rate

The possibility for runaway ions to excite Alfvénic instabilities in fusion plasmas was initially considered by Fülöp and Newton [20]. Disruption experiments at TEXTOR with massive argon injections measured increased activity of magnetic turbulence in the 60-260 kHz range [55]. We will in this section investigate whether such activity could be related to excitation of TAEs by the fast ion distribution.

It has been shown that the linearized TAE growth rate γ is given by the resonant interaction at two velocities $v = v_A/3$ and v_A [20, 54],

$$\frac{\gamma}{\omega} = \frac{2\pi^2 \mu_0 m_a^2 q_0^3 R_0}{B_0^2} \int_0^\infty \mathrm{d}v_\perp \, v_\perp \sum_{v_r = v_A/3,\, v_A} \frac{v_r}{v_A} \left(v_r^2 + \frac{v_\perp^2}{2} \right)^2 \omega \frac{\partial f_a}{\partial \mathcal{E}} \bigg|_{v_\parallel = v_r}, \tag{4.3}$$

where $q_0 = (2m+1)/2n$, (m,n) are the mode numbers of the TAE, $\omega = v_A/(2q_0R_0)$ its frequency and R_0 the major radius of the plasma. $\mathcal{E} = m_a v^2/2$ is the particle kinetic energy, and the partial derivative is taken along constant $v_\perp$. Thus,

$$\frac{\partial}{\partial \mathcal{E}} = \frac{\partial v_\parallel}{\partial \mathcal{E}} \frac{\partial}{\partial v_\parallel} = \frac{1}{m_a v_\parallel} \frac{\partial}{\partial v_\parallel}. \tag{4.4}$$

However, since the distribution given by CODION is known in terms of its Legendre decomposition $f_a = \sum_l f_l(v) P_l(\xi)$, it is convenient to express this in spherical coordinates as

$$\frac{\partial}{\partial \mathcal{E}} = \frac{1}{m_a v_\parallel} \left(\frac{\partial v}{\partial v_\parallel} \frac{\partial}{\partial v} + \frac{\partial \xi}{\partial v_\parallel} \frac{\partial}{\partial \xi} \right) = \frac{1}{m_a v} \left(\frac{\partial}{\partial v} + \frac{1-\xi^2}{v_\parallel} \frac{\partial}{\partial \xi} \right). \tag{4.5}$$

The derivative of the distribution takes the form

$$\frac{\partial f_a}{\partial \mathcal{E}} = \frac{1}{m_a} \frac{1}{v} \sum_l \left(f_l'(v) P_l(\xi) + \frac{1-\xi^2}{v_\parallel} f_l(v) P_l'(\xi) \right). \tag{4.6}$$

The integral is along the line $v_\parallel = v_r = \text{const}$, and switching to the integration variable $v = \sqrt{v_\perp^2 + v_r^2}$ yields

$$\frac{\gamma}{\omega} = \frac{\pi^2 \mu_0 m_a q_0^3 R_0 \omega}{2B_0^2} \sum_{v_r = v_A/3,\, v_A} \frac{v_r}{v_A} \sum_{l=0}^{l_{\max}} \int_{v_r}^\infty \mathrm{d}v \left(v_r^2 + v^2 \right)^2 \Bigg[f_l'(v) P_l \left(\frac{v_r}{v} \right) + \\ + \frac{1 - (v_r/v)^2}{v_r} f_l(v) P_l' \left(\frac{v_r}{v} \right) \Bigg]. \tag{4.7}$$

Integrating the f_l'-term by parts and using $P_l'(x) = l(P_{l-1} - xP_l)/(1-x^2)$, we obtain

$$\frac{\gamma}{\omega} = \frac{\pi^2 \mu_0 m_a q_0^3 R_0 \omega}{2B_0^2} \sum_{v_r = v_A/3,\, v_A} \frac{v_r}{v_A} \sum_{l=0}^{l_{\max}} \Bigg\{ -4 v_r^4 f_l(v_r) + \\ + \int_{v_r}^\infty \mathrm{d}v \left(v_r^2 + v^2 \right)^2 \left[\frac{l}{v_r} \frac{v^2}{v^2 - v_r^2} \left(P_{l-1} - \frac{v_r}{v} P_l \right) - \frac{4v}{v^2 + v_r^2} P_l \right] f_l(v) \Bigg\}. \tag{4.8}$$

We will apply this growth rate calculation to a physical disruption scenario based on the TEXTOR experiments [55], also considered by Fülöp and Newton [20]. Disruptions

were induced by injecting large amounts of argon gas, thus rapidly cooling the plasma, as previously described in subsection 4.1.2. Consistent with the experiments, we take the following parameters: magnetic field $B = 2\,\mathrm{T}$, major radius $R_0 = 1.75\,\mathrm{m}$ and carbon density $n_C = 0.042 n_D$, corresponding to a pre-disruption $Z_{\mathrm{eff}} = 2$. We consider the excitation of a low mode number wave, taking safety factor $q_0 = 1.5$. With the numerical deuterium distribution from CODION we will consider the possibility of TAEs being driven during such an event.

Since the amount of argon gas reaching the core is unknown, we will perform the calculation at various n_{Ar} with the deuterium density fixed, thus also varying the electron density. Simulations are run until the runaway ion density is $n_r = 10\%$, at which point the growth rate is calculated with Eq. (4.8). The deuterium distribution is assumed to be Maxwellian at $t = 0$, and the electric field taken to be constant.

To estimate the electric field required for runaway ions to accumulate near the resonant velocities, we can combine Eq. (2.121) for the critical velocity v_{c2} near which ions accumulate, with Eq. (2.119) for the ion critical electric field. This yields the relation

$$\frac{E}{E_c} = \frac{2}{9\sqrt{\pi}} \left(\frac{2\pi m_a}{3 m_e (Z_{\mathrm{eff}} + \bar{n})} \right)^{1/3} \frac{v_A}{v_{Te}}, \tag{4.9}$$

for the accelerated ions to reach the resonant velocity $v = v_A/3$. For $T = 25\,\mathrm{eV}$ with $Z_C = Z_{Ar} = 3$, $n_{Ar} = 0.2 n_D$ and $n_D = 1 \cdot 10^{19}\,\mathrm{m}^{-3}$, this corresponds to $E/E_c = 2.9$ when $n_{Ar} = n_D$. With such high electric fields, a significant fraction of the deuterium population will have run away before a positive velocity gradient forms. Such a scenario can not be treated consistently within our linearized model, which is valid for electric fields typically of order $E/E_c \sim 1$.

To obtain a lower value of E/E_c required to get drive, temperatures would need to be higher to increase v_{Te}, or the density of the plasma higher to decrease v_A. Increased electron density would lead to an increased critical electric field ($E_c = 26\,\mathrm{V/m}$ at the above given parameters), which would have the consequence of unrealistically high electric fields being needed to accelerate the ions. Therefore, the only way TAE drive can occur caused by pure runaway ion acceleration is if the temperature of the post-disruption plasma is significantly larger than 25 eV. We will investigate a scenario with temperature $T = 80\,\mathrm{eV}$, ion charges $Z_C = Z_{Ar} = 4$ consistent with their ionization energies [50], and also assuming a higher deuterium density $n_D = 3 \cdot 10^{19}\,\mathrm{m}^{-3}$. We will solve for the deuterium distribution function until runaway density $n_r = 10\%$, for a range of electric fields and argon densities. The resulting growth rates and the corresponding times at which they were calculated are shown in figure 4.10.

The results indicate that in the above described scenario, significant TAE growth ($\gamma > 1\,\mathrm{krad/s}$) can occur for realistic electric fields of order $30\,\mathrm{V/m}$ if a fraction of argon of at least $n_{Ar} \sim 0.2 n_D$ reaches the core, with corresponding TAE frequencies in the range $\omega/2\pi \in [50, 75]\,\mathrm{kHz}$ being in the lower range of the experimentally observed activity. In addition, theoretical models [46, 48] and experiment [47] indicate typical decay times for the electric field during a disruption of order 5 ms or less. This is not inconsistent with the time scale for significant TAE growth observed here, being as low as 3 ms.

However, static acceleration at $T = 80\,\mathrm{eV}$ is unlikely to be an accurate representation of a post-disruption plasma, which is generally expected to be significantly colder. Lower temperatures would consequently require higher electric fields to accelerate the ions. With $30\,\mathrm{V/m}$ already being a high post-disruption electric field, these considerations indicate that it is unlikely that TAEs will be driven in a TEXTOR-like plasma by runaway ions. In addition, an increased deuterium density of $n_D = 3 \cdot 10^{19}\,\mathrm{m}^{-3}$ was required to obtain a sufficiently low Alfvén velocity, which is not supported by the experiments.

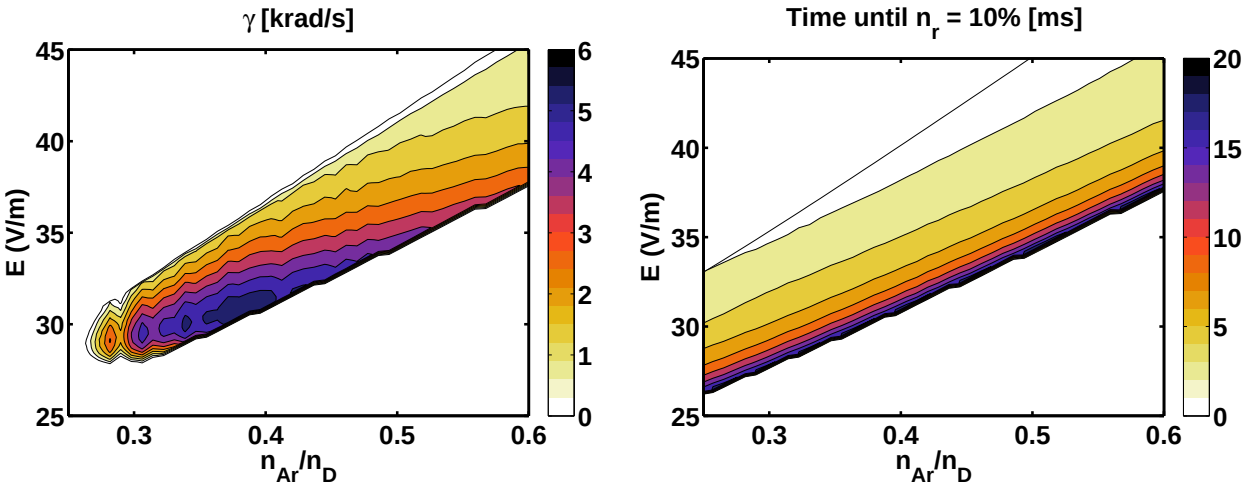

Figure 4.10: The left figure shows TAE growth rate γ and the right figure the corresponding times after which the growth rate calculation was performed. Each data point represents a calculation of γ using the deuterium distribution function, obtained from acceleration with a constant electric field from initial Maxwellian distributions, until the runaway density reaches $n_r = 10\%$ after which the growth rate is calculated. Plasma parameters assumed: temperature $T = 80\,\mathrm{eV}$ for all particle species; deuterium density $n_D = 3 \cdot 10^{19}\,\mathrm{m}^{-3}$, carbon density $n_C = 0.042 n_D$; magnetic field $B = 2\,\mathrm{T}$; major radius $R_0 = 1.75\,\mathrm{m}$; $q = (2m+1)/2n = 1.5$. The Alfvén frequency ω varies from $295\,\mathrm{krad/s}$ at $n_{Ar} = 0.6$ to $470\,\mathrm{krad/s}$ at $n_{Ar} = 0.2$.

Chapter 5

Conclusions

Acceleration of ions has long been of interest in fusion and space plasmas. Previous treatments of the problem of ion runaway have mainly been analytic, considering simplified models for ion acceleration. This has prevented previous models from obtaining many physically relevant quantities related to the fast ion distribution. A numerical solution for the ion distribution function was performed in [19] with the ARENA code, but it is not tailored for ion acceleration problems and is therefore numerically inefficient. Motivated by this, we have in this work developed an efficient numerical solver of the ion kinetic equation, allowing for strong electric fields and using a detailed collision operator. Below we will outline the main results of the investigations, and discuss possible directions of further work on the subject.

Results

A concise derivation of a two-dimensional ion kinetic equation with quasi-static electric fields has been presented. The equation includes a collision operator accounting for interactions with an arbitrary plasma background under the assumption that the deviation of other ion species from a Maxwellian equilibrium is negligible. A simplified analytical model based on the large mass ratio is used for ion-electron collisions, allowing a detailed description of ion-electron friction caused by the perturbation of the electron distribution due to the electric field. A model operator for ion self-collisions based on that used in the gyrokinetics code GS2 [33, 58] has been employed, satisfying momentum and energy conservation, non-negative entropy production and self-adjointness.

We have developed the tool CODION, based on an efficient numerical scheme for solving the ion kinetic equation. Convergence properties of the solutions have been investigated with respect to various discretization parameters, and the numerically obtained distribution functions have been benchmarked against an approximate analytic solution of the ion kinetic equation given by Fülöp and Newton [20], based on the original derivation by Helander *et al.* [19]. The effect on ion runaway of various models for self-collision operators has been investigated. It has been demonstrated that the effect of momentum and energy conservation in self-collisions is mainly an increase in the rate at which the fast ion population builds up, while the qualitative behaviour of the fast ions is largely unaffected.

Illustrative two-dimensional ion velocity space distributions have been obtained with CODION, which demonstrate the typical behaviour of runaway ions in a variety of physical scenarios. It has been demonstrated that in plasmas typical for the TEXTOR, JET and ITER tokamaks, ion runaway is unlikely to occur due to the large electric fields required to overcome collisional friction. In post-disruption plasmas it has been shown that significant amounts of runaway ions can be produced within a few milliseconds of

acceleration, although it is unlikely to occur in disruption plasmas with temperatures $T \lesssim 10\,\mathrm{eV}$ due to the low effective charge Z_{eff} of such plasmas.

We have calculated growth rates of toroidal Alfvén eigenmodes in a scenario based on massive gas injection experiments performed at TEXTOR. We have demonstrated that it is unlikely that a fast ion distribution generated primarily through electric acceleration will drive instabilities consistent with experimental observation, due to the Alfvén velocity being too high for the resonance condition to be met.

The utility of CODION has been demonstrated for calculating acceleration rates of ions in solar flare plasmas. For the first time, two-dimensional ion distribution functions have been obtained for ions accelerated by electric fields in solar plasmas. The rate at which ions are accelerated has been evaluated for a range of ion masses and charges for a solar flare scenario based on that considered by Holman [14], and an exponential decay of acceleration rate with charge for $Z > 8$ has been illustrated for this scenario.

Outlook

Multiple aspects of the model could be improved for a more complete description of the ion runaway process. In this section we will briefly discuss applications which could be further investigated, and discuss possible directions for development of the theoretical model.

Ion acceleration in solar flares: While the usefulness of CODION for the investigation of ion acceleration rates in solar flares has been demonstrated in this work, further studies are needed to compare results with experimental observations of for example energetic ion abundances in the solar wind. It would be of interest to investigate the effect of variation in parameters characterizing the flare plasma, for example plasma density, temperature, impurity content, electric field strength and acceleration time. In addition, the effect of using explicitly time-varying parameters would be of interest in the study of all scenarios considered in this work.

Knock-on collisions: One refinement of the model would be the inclusion of "knock-on", i.e. close collisions, which have been neglected in the Fokker-Planck equation. We have argued that the effect of collisions is dominantly described by small-angle collisions, giving rise to a diffusive motion in velocity space. However, single collisions can significantly change the momenta of the interacting particles, and a runaway ion interacting with a bulk ion could cause both to end up in the runaway region in a single collision event. In a situation where the electric field is low enough that runaway ions are produced at a low rate through the standard acceleration mechanism, knock-on collisions could possibly contribute significantly to the runaway generation rate. This has been demonstrated to be the case for electron runaway, where this effect drastically effects the rate at which runaways are produced [46]. A simplified runaway ion knock-on operator could potentially be constructed from the Boltzmann collision integral [24] under the assumption that fast ions accumulate near v_{c2} and collide mainly with the bulk distribution, since the fast ion distribution is assumed to be a small perturbation in our linearized model.

However, there are differences between ion runaway and electron runaway that suggest that knock-on runaway generation could be a less significant effect for ion runaway than for electron runaway: since in our linearized model we consider only cases where $E \sim E_c$, the accumulation velocity near v_{c2} will not be significantly larger than the runaway velocity v_{c1}, making an event where a runaway ion takes a bulk ion to a velocity $v > v_{c1}$ less likely, unlike the electron runaway case where the runaways have unbounded energy (neglecting radiation effects).

However, there are applications for knock-on operators other than avalanche generation. For example, it has been suggested that fast ion populations due to other sources – for example hot alpha particles created in fusion reactions, or ions heated by external sources such as NBI or RF-heating – could accelerate bulk impurity ions, which could in turn be used for diagnostics [56, 57]. The suggested collision operator could be implemented in CODION, and the time-evolution of bulk impurities solved for in the vicinity of an assumed or numerically solved for background of fast ions.

Ion-electron collisions: Another part of the model which could be improved upon is the ion-electron collision operator, for which a simplified model has been employed here. While formally valid for low electric fields, various modifications could enter in the extreme acceleration scenarios considered in this work.

The first assumption made, which could be modified in a more refined model, is that electrons reach an equilibrium state where friction against ions cancels the accelerating electric field. However, electric fields large enough to accelerate ions will also accelerate electrons. Runaway electrons will carry a net momentum, indicating that all is not transferred to ions. Simulation of accelerating electrons with CODION indicate that at most 90% of the electron momentum is transferred to the ion population in situations where ions are accelerated. Accounting for this would generally increase the accelerating effective electric field E^* for the main plasma species.

The other assumption made in this work is the neglect of the varying ion-electron friction as the fast ion population builds up. In an ion runaway scenario the fast ions will stop against friction with bulk electrons, indicating that a correction term would need to be introduced to the effective electric field, corresponding to this momentum transfer. Accounting for this could affect the latter stages of the evolution of the fast ion population, since the correction comes into play only after a significant fast ion population has formed. This may act to increase the rate at which ions are accelerated.

The first correction could in principle be accounted for by simultaneously solving for the electron distribution, calculating the momentum transfer to the ions and making the appropriate correction. The second correction could potentially be accounted for by evaluating the momentum transfer $\mathbf{R}_{ae,0}$ to the bulk electrons and adding an appropriate correction to the effective electric field. Note that both of these corrections are non-linear. The most sophisticated model for ion-electron collisions would be the simultaneous time-evolution of the ion and electron distribution functions, evaluating their corresponding Rosenbluth potentials and obtaining the full ion-electron Fokker-Planck collision operator. In the non-linear case, this would require significant modifications to the numerical implementation and likely make the algorithm significantly more computationally expensive.

Self-collisions: In this work a model operator based on that implemented in the gyrokinetics code GS2 has been employed to account for field-particle self-collisions. While the operator satisfies a range of desired physical properties, a more accurate description of self-collisions would be obtained by the full evaluation of the Rosenbluth potentials of the ion distribution.

An even more powerful model would be obtained by using the non-linear collision operator. This would allow the study of ion runaway by even stronger electric fields, since the linearized model require the fast ion population to remain a perturbation of the equilibrium state – limiting us to $E \sim E_c$. As mentioned above, this would require significant modifications to the implementation, also making the simulation computationally more expensive. In addition, at very strong electric fields the model of ion-electron collisions breaks down, requiring further modifications as outlined above.

Appendix A

Approximate analytic solution of the ion kinetic equation.

Based on the asymptotic form of the kinetic equation in the fast ion limit $v_{Ti} \ll v \ll v_{Te}$, an analytic solution for the evolution of the distribution function was originally derived by Helander *et al.* [19], for which the details of the calculation are provided below.

Consider the normalized ion kinetic equation, Eq. (3.3). For a fast ion in the regime $v_{Ti} \ll v \ll v_{Te}$, we may neglect field-particle self-collisions and use the asymptotic forms for the Chandrasekhar and error function,

$$G(x_e) = \frac{2}{3\sqrt{\pi}} x_e + \mathcal{O}(x_e^2), \tag{A.1}$$

$$G(x_i) = \frac{1}{2x_i^2} + \mathcal{O}(1/x_i^4), \tag{A.2}$$

$$\phi(x_e) = \frac{2}{\sqrt{\pi}} x_e + \mathcal{O}(x_e^2), \tag{A.3}$$

$$\phi(x_i) = 1 + \mathcal{O}\Big(\exp(-x_i^2)/x_i \Big). \tag{A.4}$$

Under the assumption that all ions have temperature T_i, the kinetic equation takes the form

$$\frac{\partial f_a}{\partial \hat{t}} + \hat{E}\left(\xi \frac{\partial}{\partial x} + \frac{1-\xi^2}{x}\frac{\partial}{\partial \xi}\right) f_a = \frac{Z_{\text{eff}}}{2x^3}\frac{\partial}{\partial \xi}\left[(1-\xi^2)\frac{\partial f_a}{\partial \xi}\right] + \frac{1}{x^2}\frac{\partial}{\partial x}\left[\left(\frac{v^3}{v_c^3} + \bar{n}\right) f_a + \frac{1}{2x}\left(\frac{T_e}{T_i}\frac{v^3}{v_c^3} + \bar{n}\right)\frac{\partial f_a}{\partial x}\right], \tag{A.5}$$

where

$$v_c = \left(\frac{3\sqrt{\pi}}{4}\frac{m_e}{m_a}\right)^{1/3} v_{Te}, \tag{A.6}$$

and $\bar{n}$ is given in Eq. (2.116). To study the initial onset of the ion acceleration process, we can neglect electron friction when compared to ion friction, assuming

$$\bar{n} \gg \frac{v^3}{v_c^3} = \frac{4}{3\sqrt{\pi}}\sqrt{\frac{m_e}{m_a}}\left(\frac{T_i}{T_a}\right)^{3/2} x^3, \tag{A.7}$$

which is approximately equivalent to the assumption $x \ll 5$. By multiplying the equation by $1/\hat{E}^{3/2}$ and defining

$$\tau = \hat{E}^{3/2}\hat{t}, \tag{A.8}$$

$$w = \sqrt{\hat{E}}x, \tag{A.9}$$

and introducing

$$F = \ln f_a \tag{A.10}$$

$$\frac{\partial f_a}{\partial x} = f_a \frac{\partial F}{\partial x}, \tag{A.11}$$

one obtains the equation for F,

$$\frac{\partial F}{\partial \tau} + \left(\xi\frac{\partial}{\partial w} + \frac{1-\xi^2}{w}\frac{\partial}{\partial \xi}\right)F = \frac{Z_{\text{eff}}}{2w^3}\left[-2\xi\frac{\partial F}{\partial \xi} + (1-\xi^2)\left(\left(\frac{\partial F}{\partial \xi}\right)^2 + \frac{\partial^2 F}{\partial \xi^2}\right)\right]$$
$$+ \frac{\bar{n}}{w^2}\frac{\partial F}{\partial w} + \frac{\bar{n}\hat{E}}{2w^4}\left(w\frac{\partial^2 F}{\partial w^2} + w\left(\frac{\partial F}{\partial w}\right)^2 - \frac{\partial F}{\partial w}\right). \tag{A.12}$$

We expand the solution in a perturbation series by writing

$$F = \ln f_a = \frac{1}{\hat{E}}F^{(0)} + \frac{1}{\sqrt{\hat{E}}}F^{(1)} + ... \tag{A.13}$$

To order $\mathcal{O}(1/\hat{E}^2)$ the equation then reads

$$0 = \frac{Z_{\text{eff}}}{2w^3}(1-\xi^2)\left(\frac{\partial F^{(0)}}{\partial \xi}\right)^2, \tag{A.14}$$

with the solution

$$\frac{\partial F^{(0)}}{\partial \xi} = 0. \tag{A.15}$$

To order $\mathcal{O}(1/\hat{E}^{3/2})$ we have

$$0 = \frac{Z_{\text{eff}}}{w^3}(1-\xi^2)\frac{\partial F^{(0)}}{\partial \xi}\frac{\partial F^{(1)}}{\partial \xi}, \tag{A.16}$$

which is automatically satisfied by the above. To order $\mathcal{O}(1/\hat{E})$ we get, using Eq. (A.15),

$$\frac{\partial F^{(0)}}{\partial \tau} + \xi\frac{\partial F^0}{\partial w} = \frac{Z_{\text{eff}}}{2w^3}(1-\xi^2)\left(\frac{\partial F^{(1)}}{\partial \xi}\right)^2 + \frac{\bar{n}}{w^2}\frac{\partial F^{(0)}}{\partial w} + \frac{\bar{n}}{2w^3}\left(\frac{\partial F^{(0)}}{\partial w}\right)^2. \tag{A.17}$$

At $\xi = 1$ this yields a non-linear equation for $F^{(0)}$,

$$w^3\frac{\partial F^{(0)}}{\partial \tau} + \left(w^3 - w\bar{n} - \frac{\bar{n}}{2}\frac{\partial F^{(0)}}{\partial w}\right)\frac{\partial F^{(0)}}{\partial w} = 0. \tag{A.18}$$

With a Maxwellian as initial distribution, we can linearize the equation for small times by writing $F = -x^2 + \delta F/\hat{E} + ... = -w^2/\hat{E} + \delta F/\hat{E} + ...$, so that

$$F^{(0)} = -w^2 + \delta F, \tag{A.19}$$

where $\delta F|_{\tau=0} \equiv 0$. The equation for $F^{(0)}$ then reads (neglecting $\mathcal{O}(\delta F^2)$ terms)

$$w^2 \frac{\partial \delta F}{\partial \tau} - 2w^3 + (\bar{n} + w^2)\frac{\partial \delta F}{\partial w} = 0. \tag{A.20}$$

For small w, the leading terms are

$$w^2 \frac{\partial \delta F}{\partial \tau} + \bar{n}\frac{\partial \delta F}{\partial w} = 0. \tag{A.21}$$

With the ansatz

$$\delta F = d(w^a + b\tau)^c, \tag{A.22}$$

we have

$$\frac{\partial \delta F}{\partial \tau} = bcd(w^a + b\tau)^{c-1}, \tag{A.23}$$

$$\frac{\partial \delta F}{\partial w} = acd(w^a + b\tau)^{c-1} w^{a-1}, \tag{A.24}$$

and the equation reads

$$cd(aw^b + \tau)^{c-1}\Big(bw^2 + a\bar{n}w^{a-1}\Big) = 0. \tag{A.25}$$

from which we obtain

$$a = 3, \tag{A.26}$$

$$b = -3\bar{n}, \tag{A.27}$$

$$\delta F = d(w^3 - 3\bar{n}\tau)^c. \tag{A.28}$$

For this to be well-defined at $w < 3\bar{n}\tau$ we can introduce the Heaviside step function $H(x)$, defined such that $H(x > 0) = 1$ and $H(x < 0) = 0$. The solution

$$\delta F = d(w^3 - 3\bar{n}\tau)^c H(w^3 - 3\bar{n}\tau) \tag{A.29}$$

will then satisfy the equation and have the correct behaviour for small velocities.

Assuming that $\partial F^{(0)}/\partial \tau$ is negligible for small τ, we can find a solution to Eq. (A.18), which then takes the form

$$\frac{\partial F^{(0)}}{\partial w} = \frac{2}{\bar{n}} w^3 - 2w, \tag{A.30}$$

with the solution

$$F^{(0)} = \frac{w^4}{2\bar{n}} - w^2. \tag{A.31}$$

The full solution is then

$$F^{(0)} = -w^2 + \frac{w^4}{2\bar{n}} + d(w^3 - 3\bar{n}\tau)^c H(w^3 - 3\bar{n}\tau), \tag{A.32}$$

and the requirement that it approaches a Maxwellian as $\tau \to 0$ gives the condition

$$0 = \frac{w^4}{2\bar{n}} + dw^{3c}, \tag{A.33}$$

yielding

$$d = -\frac{1}{2\bar{n}}, \tag{A.34}$$

$$c = \frac{4}{3}, \tag{A.35}$$

so that

$$F^{(0)} = -w^2 + \frac{1}{2\bar{n}}\Big(w^4 - (w^3 - 3\bar{n}\tau)^{4/3} H(w^3 - 3\bar{n}\tau)\Big). \tag{A.36}$$

Inserting $w = \sqrt{\hat{E}}x$ and $\tau = \hat{E}^{3/2}\hat{t}$, we finally obtain

$$f_a = \exp\left(-x^2 + \frac{\hat{E}x^4}{2\bar{n}}\left(1 - \left(1 - \frac{3\bar{n}\hat{t}}{x^3}\right)^{4/3} H(1 - \frac{3\bar{n}\hat{t}}{x^3})\right)\right). \tag{A.37}$$

This is our final expression for the time evolution of the ion distribution function, accelerated from an initial Maxwellian by an electric field, given here to leading order in the expansion parameter $\hat{E} \sim E^*/E_D$.

Bibliography

[1] J. Freidberg. *Plasma Physics and Fusion Energy.* Cambridge University Press (2007)

[2] J. Lindl. *Development of the indirect-drive approach to inertial confinement fusion and the target physics basis for ignition and gain.* Phys. Plasmas **2**, 11 (1995)

[3] M. J. Edwards *et al. Progress towards ignition on the National Ignition Facility.* Phys. Plasmas **20**, 7 (2013)

[4] S. D. Pinches. *Nonlinear interaction of fast particles with Alfvén waves in tokamaks.* PhD thesis, University of Nottingham (1996)

[5] C. Z. Cheng, M. S. Chance. *Low-n shear Alfvén spectra in axisymmetric toroidal plasmas.* Phys. Fluids **29**, 11 (1986)

[6] J. Wesson. *Tokamaks.* Oxford University Press Inc., New York (2011)

[7] J. D. Jackson. *Classical Electrodynamics.* John Wiley & Sons, Inc., Hoboken (1999)

[8] L. Landau. *On the vibrations of the electronic plasma.* J. Phys. (U.S.S.R) **10**, 25 (1946)

[9] M. N. Rosenbluth, S. V. Putvinski. *Theory for avalanche of runaway electrons in tokamaks.* Nucl. Fusion **37**, 10 (1997)

[10] T. C. Hender *et al. Progress in the ITER physics basis*, Chapter 3: MHD stability, operational limits and disruptions. Nucl. Fusion **47**, 6 (2007)

[11] A. Gibson. *Possibility of ion runaway in Zeta.* Nature **183**, 4654 (1959)

[12] A. V. Gurevich. *On the amount of accelerated particles in an ionized gas under various accelerating mechanisms.* Sov. Phys. JETP **13** (1960)

[13] E. R. Harrison. *Runaway and suprathermal particles.* J. Nucl. Energy **1**, 3 (1960)

[14] G. D. Holman. *DC electric field field acceleration of ions in solar flares.* Astrophys. J. **452** (1995)

[15] H. P. Furth, P. H. Rutherford. *Ion runaway in tokamak discharges.* Phys. Rev. Lett. **28**, 9 (1972)

[16] P. Helander, D. J. Sigmar. *Collisional transport in magnetized plasmas.* Cambridge monographs on physics (2002)

[17] M. D. Kruskal, I. B. Bernstein. *Runaway electrons in an ideal Lorentz plasma.* Phys. Fluids **7**, 3 (1964)

[18] J. W. Connor, R. J. Hastie. *Relativistic limitations on runaway electrons*. Nucl. Fusion **15**, 3 (1975)

[19] P. Helander *et al. Ion acceleration during reconnection in MAST*. Phys. Rev. Lett. **89**, 23 (2002)

[20] T. Fülöp, S. Newton. *Alfvénic instabilities driven by runaways in fusion plasmas*. Phys. Plasmas **21**, 8 (2014)

[21] L. G. Eriksson, P. Helander. *Simulation of runaway electrons during tokamak disruptions*. Comp. Phys. Comm. **154**, 3 (2003)

[22] M. Landreman, A. Stahl, T. Fülöp. *Numerical calculation of the runaway electron distribution function and associated synchrotron emission*. Comp. Phys. Comm. **185**, 3 (2014)

[23] B. A. Trubnikov. Particle interactions in a fully ionized plasma, in *Reviews of Plasma Physics 1*, edited by M. A. Leontovich. Consultants Bureau Enterprises, New York (1965).

[24] E. M. Lifshitz, L. P. Pitaevskii. *Physical Kinetics*, Volume 10 in Course of Theoretical Physics. Elsevier Ltd, Oxford (1981)

[25] F. L. Hinton. Collisional transport in plasma, in *Basic Plasma Physics I*, edited by A. A. Galeev, R. N. Sudan. North-Holland Publishing Company (1983)

[26] R. D. Hazeltine, J. D. Meiss. *Plasma Confinement*. Addison-Wesley Publishing Company, Redwood City (1992)

[27] E. Hirvijoki *et al. Guiding-center transformation of the Abraham-Lorentz-Dirac radiation reaction force*. To be submitted to Journal of Plasma Physics. Available at `http://arxiv.org/pdf/1412.1966v1.pdf`

[28] A. Stahl *et al. Effective critical electric field for runaway electron generation*. Submitted to Physical Review Letters. Available at `http://arxiv.org/pdf/1412.4608v1.pdf`

[29] A. A. Vlasov. *The vibrational properties of an electron gas*. Sov. Phys. Usp. **10**, 6 (1968)

[30] J. Decker *et al. Orbit-averaged guiding-center Fokker–Planck operator for numerical applications*. Phys. Plasmas **17**, 11 (2010)

[31] M. N. Rosenbluth, W. M. MacDonald, D. L. Judd. *Fokker-Planck equation for an inverse-square force*. Phys. Rev. **107**, 1 (1957)

[32] S. P. Hirshman, D. J. Sigmar. *Approximate Fokker-Planck collision operator for transport theory applications*. Phys. Fluids **19**, 10 (1976)

[33] I. G. Abel *et al. Linearized model Fokker-Planck collision operators for gyrokinetic simulations. I. Theory*. Phys. Plasmas **15**, 12 (2008)

[34] W. H. Press. *Numerical Recipes in Pascal: the art of scientific computing*. Cambridge Univ. Press, Cambridge (1989)

[35] T. A. Davis. *Algorithm 832: UMFPACK V4.3 – An unsymmetric-pattern multifrontal method.* ACM Transactions on Mathematical Software **30**, 2 (2004)

[36] TEXTOR, Jülich Forschungszentrum. `http://www.fz-juelich.de/iek/iek-4/DE/Forschung/10_TEXTOR/_node.html`

[37] JET, EUROfusion. `https://www.euro-fusion.org/jet/`

[38] ITER organization. `http://www.iter.org/`

[39] G. Verdoolaege *et al. Design and commissioning of a new diagnostic for routine determination of Zeff from visible bremsstrahlung measurements on TEXTOR.* Rev. Sci. Instrum. **77**, 10 (2006)

[40] S. A. Bozhenkov *et al. Disruption mitigation by massive gas injection at TEXTOR.* 34th EPS Conference on Plasma Phys., Warsaw (2007)

[41] S. A. Bozhenkov *et al. Generation and suppression of runaway electrons in disruption mitigation experiments in TEXTOR*, Plasma Phys. Control. Fusion **50**, 10 (2008)

[42] H. Smith *et al. Runaway electrons and the evolution of the plasma current in tokamak disruptions.* Phys. Plasmas **13**, 10 (2006)

[43] T. Fehér *et al. Simulation of runaway electron generation during plasma shutdown by impurity injection in ITER.* Plasma Phys. Control. Fusion **53**, 3 (2011)

[44] P. Sandquist *et al. Fast electron bremsstrahlung in low-density, grassy sawtoothing plasmas on JET.* 32nd EPS Conference on Plasma Phys. (2005)

[45] S. E. Sharapov *et al. Experimental studies of instabilities and confinement of energetic particles on JET and MAST.* Nucl. Fusion **45**, 9 (2005)

[46] P. Helander *et al. Runaway acceleration during magnetic reconnection in tokamaks.* Plasma Phys. Control. Fusion **44**, 12B (2002)

[47] E. M. Hollmann *et al. Control and dissipation of runaway electron beams created during rapid shutdown experiments in DIII-D.* Nucl. Fusion **53**, 8 (2013)

[48] G. Papp *et al. Runaway electron drift orbits in magnetostatic perturbed fields.* Nucl. Fusion **51**, 4 (2011)

[49] G. Papp *et al. Runaway electron losses caused by resonant magnetic perturbations in ITER.* Plasma Phys. Control. Fusion **53**, 9 (2011)

[50] *CRC Handbook of Chemistry and Physics, 95th edition*, edited by W. M. Haynes. CRC Press (2014)

[51] H. Smith *et al. Runaway electron generation in tokamak disruptions.* Plasma Phys. Control. Fusion **51**, 12 (2009)

[52] D. V. Reames, J. P. Meyer, T. T. von Rosenvinge. *Energetic-particle abundances in impulsive solar flare events.* Astrophys. J. **90**, 2

[53] J. T. Schmeltz *et al. Composition of the solar corona, solar wind, and solar energetic particles.* Astrophys. J. **755**, 1 (2012)

[54] T. Fülöp *et al. Finite orbit width stabilizing effect on toroidal Alfvén eigenmodes excited by passing and trapped energetic ions*. Plasma Phys. Control. Fusion **38**, 6 (1996)

[55] L. Zeng *et al. Experimental observation of a magnetic-turbulence threshold for runaway-electron generation in the TEXTOR tokamak*. Phys. Rev. Lett. **110**, 23

[56] V. G. Nesenevich *et al. Use of neutralized knock-on ion fluxes for alpha-particle confinement studies*. Plasma Phys. Control. Fusion **56**, 12 (2014)

[57] P. Helander, M. Lisak, D. D. Ryutov. *Formation of hot ion populations in fusion plasmas by close collisions with fast particles*. Plasma Phys. Control. Fusion **35**, 3 (1993)

[58] M. Barnes *et al. Linearized model Fokker-Planck collision operators for gyrokinetic simulations. II. Numerical implementation and tests*. Phys. Plasmas **16**, 7 (2009)